

AMERICAN UNIVERSITY OF BEIRUT

NEW LUMINESCENT METAL ORGANIC FRAMEWORKS
INCORPORATING HETEROTOPIC LINKERS AS CHEMICAL
SENSORS

by
RAWAN IYAD AL NATOUR

A thesis
submitted in partial fulfilment of the requirements
for the degree of Master of Science
to the Department of Chemistry
of the Faculty of Arts and Sciences
at the American University of Beirut

Beirut, Lebanon
January 2020

AMERICAN UNIVERSITY OF BEIRUT

NEW LUMINESCENT METAL ORGANIC FRAMEWORKS
INCORPORATING HETEROTOPIC LINKERS AS CHEMICAL
SENSORS

by
RAWAN IYAD AL NATOUR

Approved by:



Dr. Mohamad Hmadeh, Assistant Professor
Department of Chemistry

Thesis Advisor



Dr. Faraj Hasanayn, Professor
Department of Chemistry

Member of Committee



Dr. Digambara Patra, Professor
Department of Chemistry

Member of Committee

Date of thesis defense: 28 January 2020

AMERICAN UNIVERSITY OF BEIRUT

THESIS PROJECT RELEASE FORM

Student Name:

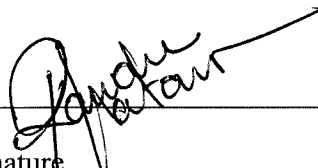
Al Natour Rawan Lyad
Middle Last First

Master's Thesis Master's Project Doctoral Dissertation

I authorize the American University of Beirut to: (a) reproduce hard or electronic copies of my thesis, dissertation, or project; (b) include such copies in the archives and digital repositories of the University; and (c) make freely available such copies to third parties for research or educational purposes.

I authorize the American University of Beirut, to: (a) reproduce hard or electronic copies of it; (b) include such copies in the archives and digital repositories of the University; and (c) make freely available such copies to third parties for research or educational purposes after:

- One ---- year from the date of submission of my thesis, dissertation, or project.
- Two ~~4~~ years from the date of submission of my thesis, dissertation, or project.
- Three ---- years from the date of submission of my thesis, dissertation, or project.



Signature Date
Rawan Al Natour 17 February 2020

ACKNOWLEDGMENTS

First and foremost, I would like to thank my thesis advisor, Dr. Mohamad Hmadeh for his continuous support for the past two years. His mentor and guidance built my confidence in research and pushed me to become a future scientist I aspire to be, working as an independent and collaborative researcher, thinking outside the box and exploring the beauty of science using my own 'eyes'. I count myself lucky to have learned a lot and it was such a pleasant experience working with him. I would also like to express my sincere gratitude for my committee members, Dr. Faraj Hasanayn and Dr. Digambara Patra, for their constructive feedback and suggestions that supported my research and provided me with insights on how I can improve my work. I would also like to thank Dr. Tarek Ghaddar, for his assistance and collaboration in providing us non-commercial linkers, and Dr. Assoud from the University of Waterloo for the single x-ray analysis which benefited a lot my research. I would also like to extend a heartfelt gratitude to the Central Research Science Laboratory (CRSL), especially Ms. Rania Shatila, for her training and support which was an integral part in finishing my thesis. As a member in Dr. Hmadeh's research group, I would like to acknowledge the priceless collaborative and daily mental and academic support provided by my colleagues, Mahmoud, Ghiwa and Zeinab and on the side Meghry! I am not sure if my family is going to read this, but words cannot express my deepest and sincere gratefulness for having them by my side this whole journey. An earnest thanks to my Mom and Dad who inspired me to pursue my master's degree and encouraged me to continue following my dream. Without their support, I would not have been where I am today. Last but not least, I am very grateful for my sister and brother whom I know will support me unconditionally until my last breath.

AN ABSTRACT OF THE THESIS OF

Rawan Iyad Al Natour for Master of Science
Major: Chemistry

Title: New Luminescent Metal Organic Frameworks (MOFs) Incorporating Heterotopic Linkers as Chemical Sensors

Metal–organic frameworks, known as MOFs, are hybrid robust materials constructed from metal centers and organic linkers. The topicity of linkers used plays an important role in the predetermination of the structural attributes, properties and functionalities of MOFs. The earliest MOFs reported are composed of homotopic linkers, mainly attributed to their high symmetry and identical functional groups, which enables uniformity and homogeneity within the framework. On the other hand, the incorporation of heterotopic linkers (i.e. linkers containing more than one type of coordinating group) has long been an ongoing challenge. Apart from being non-symmetric, the uncertain coordination of all functional groups is the main obstacle faced in integrating heterotopic linkers in MOFs. However, it is more common that the different coordination groups incorporated tend to serve different limitations upon their incorporation within the MOFs structure. For instance, one coordinating unit acts to direct the geometry, structure and binding confinement; while other types of coordinating units act to complement functional assets of the framework.

This thesis explores the integration of heterotopic linkers within two different and novel MOF structures having two different chelating groups; carboxylate and pyridine functional units and investigates its effects on its ability of luminescent sensing. The preparation, characterization methods and the MOF-guest interactions resulting in luminescent sensing are covered.

The first structure integrates a rather simple heterotopic linker, 1,4-pyridinecarboxylic acid, known as isonicotinic acid (having one pyridine and one carboxylate functional units) and Cu(II) metal center to yield a 2-dimensional (2D) layered metal–organic framework that is subsequently exfoliated into its complementary nanosheets and subjected cation and solvent sensing applications.

The second structure assimilates a more complex heterotopic linker, 2,2':6',2''-terpyridine-4'-carboxylic acid, which includes terpyridine and one carboxylate functional units, in coordination with Cu(II) metal center to yield a new 1-dimensional (1D) framework.

CONTENTS

ACKNOWLEDGEMENTS.....	V
ABSTRACT.....	VI
ABBREVIATIONS	X
LIST OF ILLUSTRATIONS.....	XII
LIST OF TABLES.....	XV

Chapter

I. RETICULAR CHEMISTRY– STRUCTURE, PROPERTIES AND APPLICATIONS OF METAL– ORGANIC FRAMEWORKS

A. Emergence of metal–organic frameworks.....	2
B. Structural components of metal–organic frameworks.....	4
1. Secondary Building Units.....	5
2. Organic Linkers.....	7
C. Multi-component metal–organic frameworks.....	10
1. Isorecticular metal–organic frameworks.....	10
2. Heterogeneity in homotopic linkers.....	12
3. Heterogeneity in heterotopic linkers.....	15
4. Multivariate metal–organic frameworks.....	17
i. Multi-Metal MTV-MOF.....	17
ii. Multi-Metal MTV-MOFs.....	17
D. Luminescent metal–organic frameworks.....	19
1. Linker-based emission.....	20
2. Framework metal ions.....	21

3. Encapsulated luminophores.....	22
OBJECTIVES.....	25
II. MATERIALS AND METHODS	
A. Synthesis of AUBM-6.....	26
B. Synthesis of 2,2':6',2''-terpyridine-4'-carboxylic acid (cterpy) ligand.....	27
C. Synthesis of AUBM-7.....	27
D. FT-IR measurements.....	28
E. Thermogravimetric analysis.....	28
F. Single Crystal X-ray Diffraction.....	28
G. Powder X-ray Diffraction.....	28
H. Scanning Electron Microscopy.....	29
I. Brunauer–Emmett–Teller (BET) surface area measurement.....	29
J. UV-Vis spectroscopy.....	29
K. Fluorescence spectroscopy.....	29
L. Solvent titrations.....	30
M. Metal ions titrations.....	30
III. SYNTHESIS, CHARACTERIZATION AND APPLICATION OF TWO-DIMENSIONAL METAL–ORGANIC FRAMEWORK AUBM-6	
A. Introduction.....	31
B. Results and Discussion.....	33
1. Description of Crystal Structure.....	33
2. PXRD Patterns and Thermogravimetric Analysis.....	37
3. FT-IR spectrum analysis and BET surface area measurement.....	37

4. Effect of exfoliation on PL-spectra of AUBM-6.....	42
5. Ratiometric selectivity towards acetone.....	46
6. PL-spectra of AUBM-6-NS “turn-off” towards Pd ²⁺	46
C. Conclusions.....	52
 IV. SYNTHESIS AND CHARACTERIZATION OF NEW ONE-DIMENSIONAL METAL–ORGANIC FRAMEWORK AUBM-7	
A. Introduction.....	54
B. Results and Discussion.....	56
1. Description of Crystal Structure.....	56
2. Powder X-ray Diffraction and Thermogravimetric Analysis.....	58
3. Scanning Electron Microscopy of AUBM-7.....	59
4. Uv-vis and Fluorescence Spectroscopy.....	60
C. Conclusions.....	61
 V. CONCLUDING REMARKS AND FUTURE PERSPECTIVES.....	
REFERENCES.....	65

ABBREVIATIONS

MOF Metal–Organic Framework

PCP Porous Coordination Polymer

BIPY Bipyridine

CCDC The Cambridge Crystallographic Data Center

CSD Cambridge Structural Database

SBU Secondary Building Unit

BDC Benzene-1,4-dicarboxylic acid

BPZ 3-pyrazol-3-ylidenepyrazole

DMF Dimethyl formamide

IR-series Isorecticular series

BTB 4,4',4''-benzene-1,3,5-triyl-tribenzoate

BPDC Biphenyl-4,4'-dicarboxylate

BTE 4,4',4''-(benzene-1,3,5-triyl-tris(ethyne-2,1-diyl)) tribenzoate

TPA 4,4',4''-nitriлотribenzoate

TMTMPC 2',3',5',6'-tertramethylterphenyl-4,4''- dicarboxylate

H₂PyC 4-pyrazolecarboxylic acid

MTV-MOF Multivariate Metal–Organic Framework

DOT Dioxidoterephthalate

MLCT Metal-to-Ligand Charge Transfer

LMCT Ligand-to-Metal Charge Transfer

DABCO 1,4-diazabicyclo [2.2.2]octane

INA 4-pyridinecarboxylic acid

Cterpy 2,2':6',2''-terpyridine-4'-carboxylic acid

NMP N-methyl-2-pyrrolidone

AUBM-6 American University of Beirut Materials

AUBM-6-NS American University of Beirut Materials Nanosheets

FT-IR Fourier-Transform Infrared Spectroscopy

TGA Thermogravimetric Analysis

PXRD Powder X-ray diffraction

SEM Scanning Electron Microscope

BET Brunauer–Emmett–Teller surface area measurement

DCM Dichloromethane

DMA Dimethylacetamide

THF Tetrahydrofuran

PL Photoluminescence

ILLUSTRATIONS

Figure	Page
1.1 Progression of the MOF entries in the Cambridge Structural Database from 1972 to 2016. Inset: Scheme depicting the constructive process of MOFs from secondary building units (red) and organic linkers (blue).....	4
1.2 Different examples of SBUs formed via carboxylate functionalized MOFs. The inorganic units representing metal-oxygen polyhedra are blue, and the polyhedron defined by carboxylate carbon atoms are red. The organic counterparts represented by polygons indicating the direction through which linkers are extended are shown in green. Oxygen (red); Nitrogen (green); Carbon (black).....	6
1.3 Binding modes of R-COO- to metal centers.....	7
1.4 Organic linkers of similar lengths bearing different coordinating groups yield two different secondary building units leading to different framework structures (BDC = 1,4-benzene dicarboxylic acid; BPZ = bipyrazole).....	9
1.5 Coordination of same organic linker (BDC= 1,4-benzenedicarboxylate) and zinc nitrate under different reaction conditions yield two different secondary building units with two different framework structures. Zinc (blue), Oxygen (red), Carbon (black).....	10
1.6 Single crystal structures of IRMOF-n (n=2, 3, 4, 10, 14 and 16) obtained by combining Zn ₄ O cluster with different ditopic linkers. Zn cluster (blue polyhedron), Carbon (black), Oxygen (red), porous voids (large yellow spheres).....	11
1.7. Crystal structures of (a) UMCM-1 (b) MOF-210 and (c) UMCM-12 which are composed of di- and tri-topic linkers connected to a Zn ₄ O(COO) ₆ SBU. Zn ₄ O(COO) ₆ (blue polyhedron); Oxygen (red); Carbon (black). The large yellow and orange spheres represent the different voids occupying the cavities of MOFs.....	15
1.8 Incorporation of heterotopic linker (H ₂ PyC = 4-pyrazolecarboxylic acid) yields different SBUs producing multi-component MOFs. Copper (yellow); Zinc (aqua), Nitrogen (blue), Oxygen (red); Carbon (black). The large yellow and orange spheres represent the different voids occupying the cavities of MOFs.....	16
1.9 MTV-MOF-5 with various functionalized organic linkers incorporated within the same structure (left), MTV-MOF-74 of different metal ions SBUs (right).....	19
1.10 Scheme depicting emission possibilities in a porous MOF.....	23
2.1 Synthesis route of AUBM-6 crystals starting from INA ligand.....	26

2.2 Synthesis route of AUBM-7 crystals starting from cterpy ligand.....	27
3.1 (A) Multi-layer view of the 1D channels of AUBM-6 (C ₁₇ H ₁₇ CuN ₃ O ₆). (B) Coordination mode dimensions of AUBM-6. (C) Coordination environment of the Cu ²⁺ ion in AUBM-6. (D)(E) 2D multi-layer side view of AUBM-6. Copper (gold); Oxygen (red); Nitrogen (green), Carbon (black).....	36
3.2 (A) Simulated and experimental PXRD patterns of AUBM-6 and AUBM-6-NS before and after acetone and Pd ²⁺ sensing (B) Thermogravimetric analysis of AUBM-6.....	37
3.3 FT-IR spectrum of INA ligand and AUBM-6.....	38
3.4 BET surface area measurement curve of AUBM-6.....	39
3.5 SEM images of (A) Bulk crystals of AUBM-6 (B) Single crystal of AUBM-6 (C)(D) Layered morphology of AUBM-6 (E)(F) Exfoliated few layer nanosheets of AUBM-6-NS.....	40
3.6 (A) UV adsorption spectrum of blank acetone (blue) and excitation spectrum of AUBM-6 (black) (B) UV-Vis Spectrum of INA ligand and AUBM-6 in acetonitrile CH ₃ CN.....	41
3.7 PL-spectra of INA, AUBM-6 and AUBM-6-NS in acetone at $\lambda_{\text{ex}} = 285$ nm.....	41
3.8 (A) PL-spectra of AUBM-6-NS upon addition of different organic solvents (2.0 vol%) at 1000 μl . (B) Ratiometric probe of AUBM-6-NS initially dispersed in CH ₃ CN upon gradual titration with acetone at (1) 0 μl and (2) 1000 μl . Inset: Intensity ratio at 409 nm and 317 nm PL emission of AUBM-6-NS upon addition of different amounts of acetone (at $\lambda_{\text{ex}} = 285$ nm).....	43
3.9 Fluorescence intensity versus time trajectories of AUBM-6-NS upon continuous excitation at $\lambda_{\text{ex}} = 285$ nm.....	45
3.10 Reversibility of ratiometric peaks upon gradual increase in temperature from (1) 25 °C (2) 30 °C (3) 35 °C (4) 40 °C (5) 45 °C (6) 50 °C at $\lambda_{\text{ex}} = 285$ nm. Inset: Colorimetric changes of AUBM-6-NS in (i) acetone under visible light (ii) acetonitrile under ultraviolet light (iii) acetone under ultraviolet light. (B) Recyclability of the ratiometric peaks of AUBM-6-NS after temperature increase (pink: I ₃₁₇) and (blue: I ₄₀₉).....	46
3.11 (A-B) PL quenching intensities of different metal cations upon addition of 0.8 ppm at $\lambda_{\text{ex}} = 285$ nm. (C) PL spectra of AUBM-6 upon gradual titrations at (1) 0 ppm and (2) 0.8 ppm of Pd ²⁺ ions at $\lambda_{\text{ex}} = 285$ nm. Inset: Stern-Volmer plot demonstrating gradual	

Pd ²⁺ titrations (D) Colorimetric changes of AUBM-6-NS in solution upon addition of 0.8 ppm of different metal cations.....	47
3.12 Effect of exfoliation on sensing Pd ²⁺ at 0.8 ppm of AUBM-6-NS and AUBM-6.....	49
3.13 The change in fluorescence intensity of AUBM-6-NS in acetone upon addition of (A) As ³⁺ (B) Fe ³⁺ (C) Zn ²⁺ (D) Cr ³⁺ followed by 0.8 ppm Pd ²⁺ solution.....	50
3.14 (A)(B)(C) Control experiments upon the addition of 700 μl pure solutions without Pd ²⁺ ions (D)(E)(F) Quenching experiments having Pd ²⁺ ions in corresponding pH solutions upon addition of (1) 0 μl (2) 700 μl.....	51
3.1 Proposed pathway of the quenching mechanism of AUBM-6-NS upon the addition of Pd ²⁺ ions. Copper (gold); Oxygen (red); Nitrogen (green), Carbon (black).....	52
4.1 2,2':6',2"-terpyridine (left) 2,2':6',2"-terpyridine-4'-carboxylic acid (right).....	55
4.2 (A) Crystal 1-dimensional structure of AUBM-7 (B) Coordination environment and reverse orientation of subsequent multi-layers of AUBM-7 (C) One-dimensional coordination route of AUBM-7 along b-axis (D) Multi-layer view of AUBM-7 (E) π-π stacking of AUBM-7. Copper (gold); Oxygen (red); Nitrogen (green); Carbon (black); Chloride (yellow).....	57
4.3 (A) PXRD patterns of simulated and as-synthesized samples of AUBM-7 (B) TGA of AUBM-7 between temperature range 30-1000°C.....	59
4.4 SEM images of : (A) single crystal of AUBM-7 ; (B) top view of AUBM-7 single crystal; (C) and (D) multilayers topology of AUBM-7.....	60
4.5 Absorption spectrum of AUBM-7 and emission spectra of AUBM-7 and free cterpy ligand at λ _{ex} = 270 nm.....	61

TABLES

Table	Page
3.1 Crystal data and structure refinement of AUBM-6.....	35
3.2 Literature survey about previously reported MOFs towards acetone sensing.....	44
3.3 Literature survey about previously reported chemo-sensors towards Pd ²⁺ sensing. PA: Picric acid; NA: Not applicable.....	48
4.1 Crystal data and structure refinement of AUBM-7.....	57

CHAPTER I

RETICULAR CHEMISTRY– STRUCTURE, PROPERTIES AND APPLICATIONS OF METAL–ORGANIC FRAMEWORKS

Overview

The chemistry of linking molecular building blocks by strong bonds to make crystalline open frameworks, also known as reticular chemistry, has significantly taken a high toll in expanding the scope of chemical compounds and materials.¹ In essence, reticular synthesis is known for the judicious geometry assembly of rigid molecular building blocks into strongly bonded predetermined ordered networks.² There are two basic aspects that define the core of reticular chemistry, which impacts the linking route of molecular building units by strong bonds to make large crystalline and extended structures. The first is concerned with the directionality and type of interactions readily existing within linkages, and the second pertains to the geometry of the molecular building units which plays an important role in guiding the length, size and angles to a specific structure.³ Specifically, metal–organic frameworks (MOFs) exemplify the means by which this chemistry is practiced and controlled at molecular level. MOFs are typically constructed from metal nodes adjoined by organic linkers through strong bonds; where the variation of the combination of metal ions and organic linkers achieves a wide spectrum of desired structures and compositions.¹⁻³ Nevertheless, with the immense diversity that can be created, it remains an ongoing challenge to control the spatial arrangement of ligands' geometry around the metal nodes. Although the synthesis of new materials has long been referred to by critics as “shake and bake” or

“heat and beat”, it mostly remains more of an art than science, in which the urgency to design materials exhibiting highly specific functions is elevating.

A. Emergence of metal–organic frameworks

The field of coordination chemistry as it is practiced today has been known to be the origin of synthetic metal–organic chemistry.³ Little known about their structure and composition, early examples of transition metals were discovered by chance centuries ago.⁴ Swiss chemist, Alfred Werner, laid the conceptual foundation for modern coordination chemistry for transition metals in 1893, in which he contradicted the theory of constant valence and proposed that transition metals can withhold different geometries according to their different coordination numbers and oxidation states.⁵ Furthermore, Werner’s work inspired Karl A. Hoffman in 1897 to extend the practice of coordination chemistry from the molecular regime (0D) into higher structural dimensions, specifically 2D and 3D extensions.⁶ Commonly referred to as Hoffman’s clathrate, the slow diffusion of C₆H₆ into an NH₃ solution of Ni(CN)₂ demonstrates an early example of coordination compound having an extended 2D structure with a crystalline composition. A variety of subsequent Hoffman clathrate compounds demonstrating extended structures have been reported, in which the substitution of ammonium ligands with alkylamines have been employed.⁷ The introduction of alkylamines between the adjacent 2D layers of Hoffman clathrate facilitated the fixation of the interlayer distance and enhanced its properties, thus extending it into a 3D coordination compound. The next logical progression to incorporate organic linkers entirely to metal ions to form various metrics of extended structures of coordination networks was reported by Richard Robson.⁸ The linkage of metal centers through organic struts lead to the formation of frameworks encompassing open space where

weak interactions including hydrogen bonds, halogen bonds, π -interactions, and Van der Waals forces existed between individual molecules, thus contributing in the arrangement within the crystal. It is however worthy of note that at this point, the geometric design and level of synthetic control principles were largely unknown.

The past few decades withheld a myriad of solids being characterized by having metal ions linked by molecular species termed as hybrid organic–inorganic materials, organic zeolite analogues and porous coordination polymers (PCPs).⁹⁻¹⁰ Although each term carries its own connotation with regards to the compound it encompasses and its composition; the term metal–organic framework (MOF) was originally used by Omar M. Yaghi and co-workers in 1995 who reported the solvothermal synthesis of $[\text{Cu}(\text{BIPY})_{1.5}](\text{NO}_3)$ (BIPY = bipyridine) to describe the over-all composition (metal ion and organic counterpart)¹¹. In more recent years, additional structural attributes (rigidity) and properties (porosity) were meaningfully employed to describe MOFs. In 2016, according to The Cambridge Crystallographic Data Center (CCDC) the estimated number of MOFs discovered with diverse topologies exceeded 70,000 out of the 850,000+ structures reported in the Cambridge Structural Database (CSD) in the past 40 years (**Fig. 1.1**).¹² Hence, for a solid to be considered a metal-organic framework, it should exhibit a strong bonding strength yet flexible and dynamic, geometrically well-defined topology, presence of accessible pores for guest molecules, highly crystalline structure and capability for post modification via organic syntheses¹³. The conceptual approach adopted by MOFs relies on the network connectivity of its building units that largely determines its properties, which include the definition of the size of available porous channels or the inclusion of chiral centers or reactive sites within the open framework.¹³

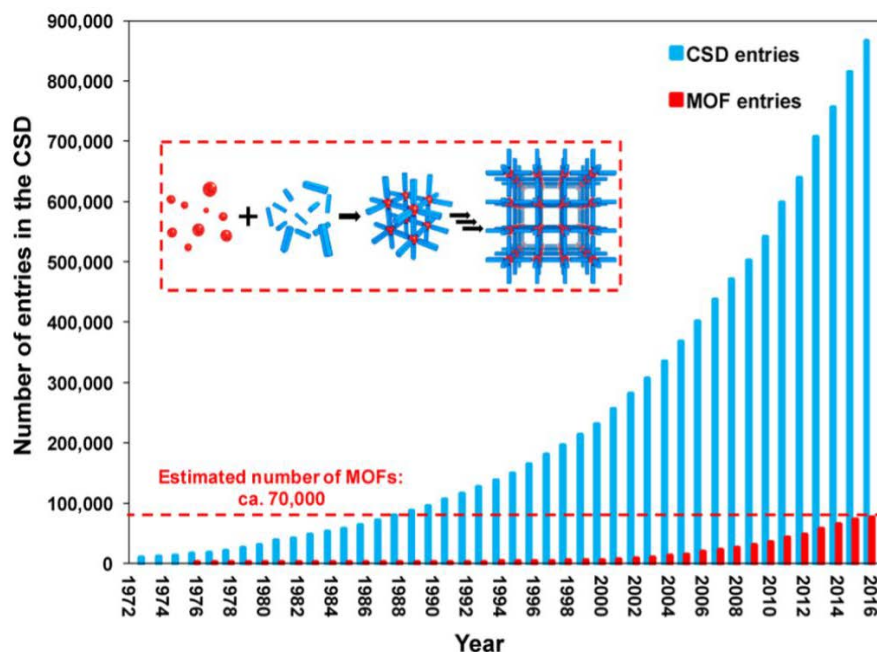


Figure 1.1 Progression of the MOF entries in the Cambridge Structural Database from 1972 to 2016. Inset: Scheme depicting the constructive process of MOFs from secondary building units (red) and organic linkers (blue).¹²

B. Structural components of metal–organic frameworks

In order to determine the assembly route of MOFs based on underlying nets constructed via linked vertices or edges, its' structure has to be deconstructed into individual building units. Such building blocks are dissected into inorganic and organic components, which are commonly referred to secondary building units (SBUs) and linkers, respectively.¹⁴ Linkers bear binding groups such as carboxylates, phosphates, pyrazolates, tetrazolates, catecholates, and imidazolates to form extended framework structures with various properties; however, carboxylate functionalized MOFs comprise by far the largest group owing to their chelating nature, which favours the formation of polynuclear metal–carboxylate SBUs. Such SBUs, provide strong bonding between constituents, directionality and high mechanical, architectural and chemical stability.¹⁴

1. Secondary Building Units

Secondary building units (SBUs), also known as polynuclear cluster nodes, are molecular complexes in which multidentate linkers such as carboxylates are utilized to aggregate metal ions into M–O–C clusters.¹⁵ Such SBUs are considered to be sufficiently rigid due to the carboxylates' ability to “lock” the metal ions into their respective positions via strong covalent directional bonds.¹⁶ The concept of secondary building units (SBUs) as structure entities were adopted in order to aid the process of structure prediction.¹⁷ For instance, defined by simple geometric figures of the inorganic clusters or coordination spheres, SBUs exhibit branching points that are commonly encountered in metal–carboxylate MOFs. The latter polynuclear cluster nodes are linked by organic ligands from their respective extension points to form the product framework. As it can be seen in **Figure 1.2**, metal–oxygen forming the inorganic cluster unit are denoted by the blue polyhedra. The carboxylate carbon atoms adjoining the inorganic moieties (denoted by black) form the points of extension that link one or more organic ligands yielding various structural frameworks. It is worthy to note that these complex SBUs are not commonly introduced directly as molecular species, but are rather formed in situ under specific synthetic conditions, where the metal ions and linkers are mixed solvo- or hydro-thermally (one-pot synthesis strategy), which allows for the slow and irreversible assembly of the overall frameworks and consequently leads to the formation of highly crystalline frameworks.¹⁸⁻¹⁹ In contrast, by varying synthesis conditions, SBUs, such as Zirconium clusters, have been reported to be isolated prior its assembly with organic linkers, allowing for diversity of clusters, hence topology predetermination.²⁰⁻²¹

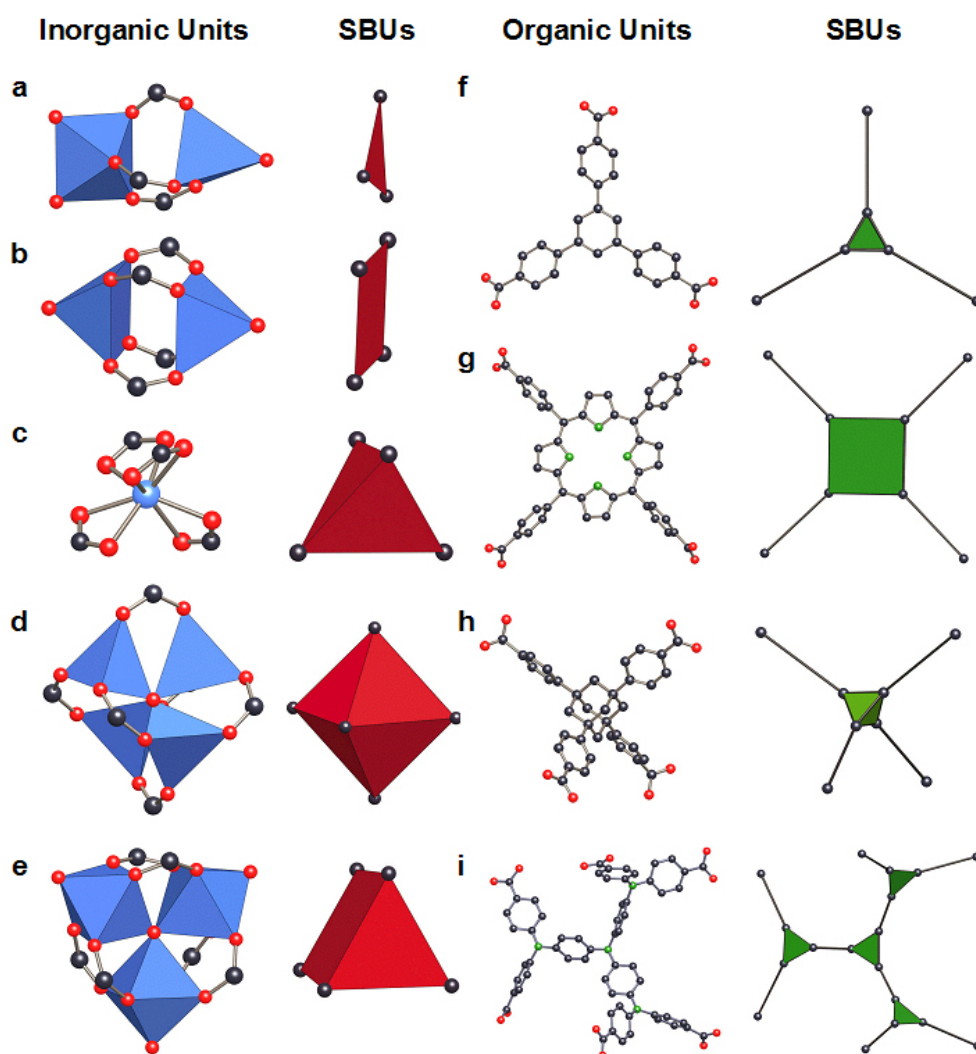


Figure 1.2 Different examples of SBUs formed via carboxylate functionalized MOFs. The inorganic units representing metal-oxygen polyhedra are blue, and the polyhedron defined by carboxylate carbon atoms are red. The organic counterparts represented by polygons indicating the direction through which linkers are extended are shown in green. Oxygen (red); Nitrogen (green); Carbon (black).²

Adjoining a network of organic linkers at large rigid vertices instead of having it at one metal ion vertex, SBUs have the advantage to produce extended frameworks of high structural, chemical and thermal stability. In contrast to single metal nodes, the diverse geometries and increased connectivity of such SBUs make them ideal building units for accessing a substantial variety of framework structures with predictable functionalities. By analyzing specific synthesis and reaction conditions toward SBU production, it is

important to understand the coordination chemistry of R–COO–M in order to target a degree of certainty toward the final SBU geometry. In the SBU structures of carboxylate-based MOFs, the binding nature of carboxylates to metal centers vary from ionic bonds, unidentate, symmetric and asymmetric chelating and bridging modes (**Figure 1.3**). Such binding modes strongly depend on the nature of the metal favouring its coordination; nevertheless, the predominant coordination relies within chelating and bridging modes as they favour the formation of polynuclear clusters.²²⁻²³

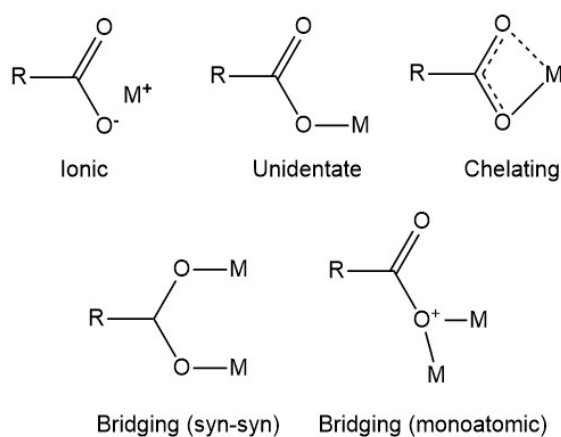


Figure 1.3 Binding modes of R–COO– to metal centers

2. Organic linkers

In the mid-1990s, bipyridines and nitriles were initially used as neutral donor linkers to prepare coordination networks.³ Nevertheless, such materials were thermally and chemically nonstable due to their monodentate coordination nature. Additionally, knowing that neutral pyridine ligands tend to form positively charged frameworks, its drawback relies in having counter ions occupying the pore space in MOFs, thus limiting their utility and functionality. In contrast, carboxylate-based linkers, having a charged binding group, later replaced such linkers due to their advantageous properties over neutral donor linkers which include:²⁴⁻²⁵

- i. Their ability to neutralize positive charges present on the metal ion clusters without the need of counterions, thus forming neutral frameworks
- ii. Their chelating nature that provides structural stability, rigidity and directionality due to the metal–oxygen–carbon clusters (SBUs)
- iii. Their distinct functional group favour the formation of polynuclear clusters (SBUs) with fixed connectivity and coordination geometry due to the carboxylate carbons which act as points from where the MOF will extend
- iv. Their strong bonding strength toward the metal centers of the SBUs result in MOFs having higher thermal, chemical and mechanical stability

Coordinating groups other than carboxylates were also investigated by researchers with success. Expanding the scope of linkers which bear varying types of functional coordinating groups remains a valuable endeavour in determining the structural properties, stability and functionality of MOFs. For instance, the variation of linkers with different coordination groups with the same metal ion source and the same reaction conditions yields various SBUs.²⁶ As it can be seen in **Figure 1.4**, the reaction of Zn^{2+} with pyrazole linker yields a chain-like SBU while its reaction with carboxylate linker having roughly equal length produces the well-known octahedral cluster $\text{Zn}_4\text{O}(\text{-COO})_6$ present in MOF-5. These coordinating functionalities exhibit differences in charge, basicity or acidity, flexibility and chelating ability which either affect the coordination environment around the metal cluster or the adopted geometry of the coordination sphere.

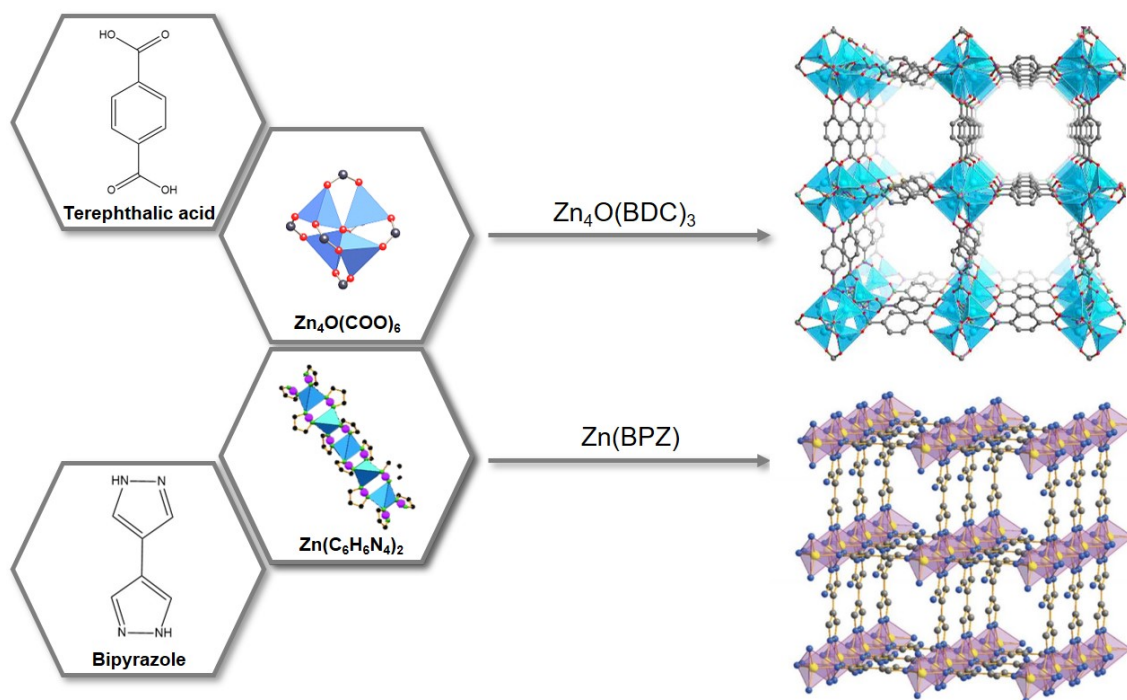


Figure 1.4 Organic linkers of similar lengths bearing different coordinating groups yield two different secondary building units leading to different framework structures (BDC = 1,4-benzene dicarboxylic acid; BPZ = bipyrazole).

On the other hand, using the same metal ion source and organic linker under different reaction conditions also serves the variation in the structural attributes of MOFs.²⁷ In the case of employing terephthalic acid (BDC) as a main organic linker and zinc nitrate as main metal ion source, two different secondary building units are formed, yielding two different framework structures. In particular, MOF-2 was reported in 1998 and initially synthesized from a mixture of DMF (dimethylformamide) and H_2O , having the formula $Zn(BDC)(H_2O)$ (BDC= 1,4-benzenedicarboxylate).²⁸ The MOF structure is composed of $Zn_2(COO)_4$ paddlewheel SBU interlinked by BDC linkers, resulting in a 2D microporous layered network (**Fig. 1.5**). Interestingly, under different reaction conditions (DMF), a different SBU resulted as it is observed in the case of MOF-5; whereby the well-known represented cluster entity is composed of a tetrahedral central oxide unit surrounded by four different Zn^{2+} ions and coordinated by a total of six

bridging $-\text{COO}$ groups.²⁹ Unlike the structure of MOF-2, the resulting framework represents a cubic 3D coordination network.

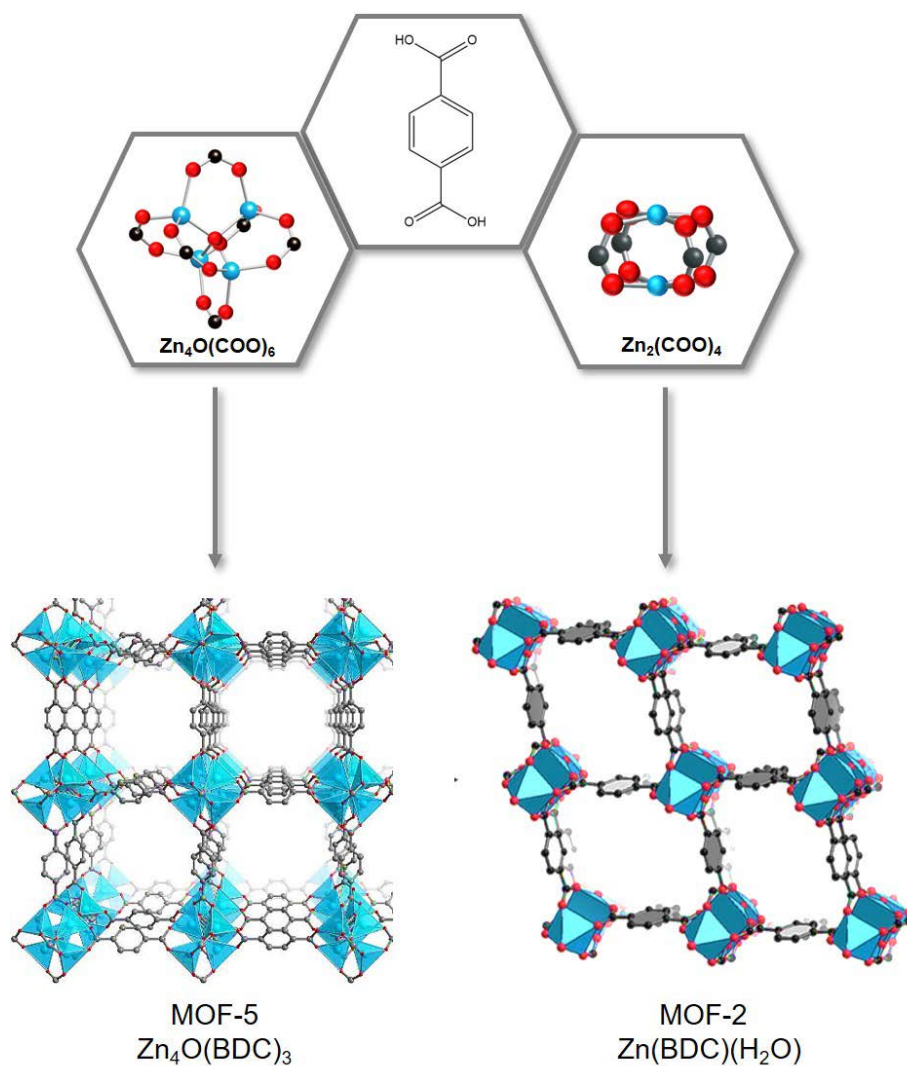


Figure 1.5 Coordination of same organic linker (BDC= 1,4-benzenedicarboxylate) and zinc nitrate under different reaction conditions yield two different secondary building units with two different framework structures. Zinc (blue), Oxygen (red), Carbon (black).

C. Multi-component metal–organic frameworks

1. Isorecticular metal–organic frameworks

The determination of topology and porosity of MOFs is exclusively correlated to the metrics and functionality of such solid-state materials, specifically their sorption properties. It is still a challenge to obtain MOFs with a predetermined pore size;

nevertheless, it is a greater challenge to synthesize MOFs with various pore sizes without modifying the topology of the parent framework. Hence, the elongation or functionalization of organic linkers under similar synthetic conditions with the same coordination environment of SBUs results in an isorecticular (IR) series of MOFs. One of the first successful implementations of IR-series is demonstrated via MOF-5 topology (**Fig. 1.6**) where the expansion and functionalization of ditopic carboxylate linkers, specifically BDC, reticulated with $Zn_4O(COO)_6$ cluster yielded MOFs having the same cubic topology, yet with various pore sizes or functionalities.³⁰

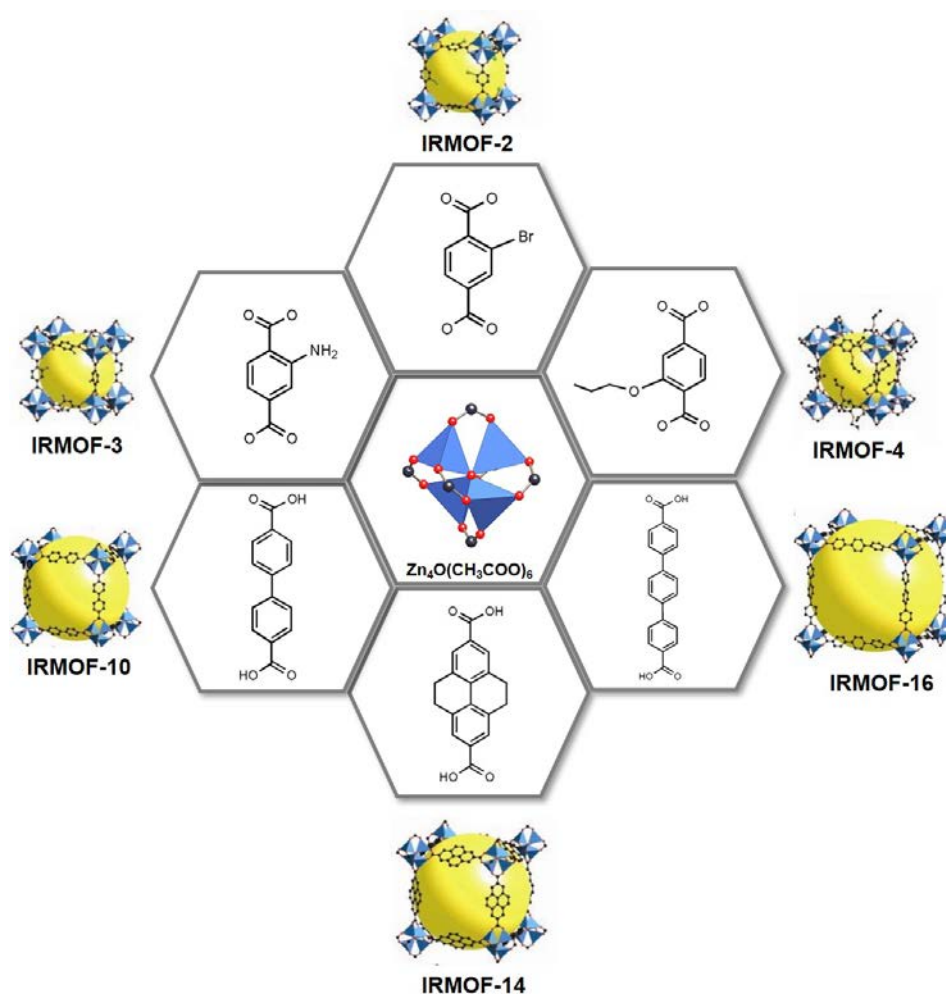


Figure 1.6 Single crystal structures of IRMOF-n (n=2, 3, 4, 10, 14 and 16) obtained by combining Zn_4O cluster with different ditopic linkers. Zn cluster (blue polyhedron), Carbon (black), Oxygen (red), porous voids (large yellow spheres)

For instance, as it can be seen in IRMOF-2 through -7, incorporating functionalized BDC links with bromo, amino, n-propoxy, n-pentoxy, cyclobutyl, and fused benzene functional groups result in the same MOF-5 skeleton; however, with the various functional groups pointing towards the voids, hence adding various functional properties to the framework. Consequently, illustrations of IRMOF-8 through -16 show the successive expansion of the parent framework by using progressively extended links, by which aperture sizes of isostructural MOFs ranged from 3.8 to 19 Å. Such modifications remain rarely seen in crystalline solid state and porous materials research. On the other hand, undergoing the expansion of MOFs from the microporous (pore diameter < 2 nm) to the mesoporous (pore diameter > 2 nm) regime with higher pore diameters is advantageous in large-molecule applications. Nevertheless, such expansions subject the modified pores either to lose significant accessible surface areas during solvent removal/exchange resulting in distortion of the MOF's structure or collapse of the framework upon activation.³¹⁻³³ Therefore, recent advances have resorted towards a solution which allows the hybridization of guest polymers with MOFs to enhance the framework's mechanical stability and maintain its porosity upon harsh activation conditions.³⁴⁻³⁷ For instance, the insertion of small polymer guests such as polydopamine into the mesoporous channels as pillars have been recently reported, which act to pin the mesoporous channels open during subsequent harsh activation process, thus preventing the pores from collapsing and leaving them accessible to gas molecule applications.³⁸

2. *Heterogeneity in homotopic linkers*

On another note, a large number of linkers employed during the synthesis of MOFs possess relatively high symmetries mainly due to their identical connectivity of the

functional groups to the rigid unsaturated hydrocarbon fragment. The basic geometries of organic linkers predetermine the points of extensions that will be connected within the SBUs, ranging from 2, 3, 4, 6, 8 to 12.³⁹ Points of extensions are the points that connect one SBU to another via organic linkers. Consequently, the terminologies used to describe them: ditopic, tritopic, tetratopic and so on emerge. Depending on the binding modes, the linkage of such organic linkers with the metal clusters results in a one-, two- or three-dimensional crystalline network. In one-dimensional (1D) MOFs, coordination bonds extend in one direction, while in two- and three-dimensional (2D, 3D) MOFs, bonds extend in two and three dimensions respectively. The choice of linkers; however, whether being homotopic (same type of coordination sites) or heterotopic (different type of coordination sites), results in variations within the linkage of the MOF's components. For instance, incorporating homotopic organic linkers facilitates crystallization due to its high symmetry ends and identical coordination sites, which in return enables uniformity of a coordinating group.⁴⁰ Without regards to the type of coordinating group incorporated, nearly most MOFs are composed of homotopic linkers. Heterotopic linkers bearing at most two different types of coordinating groups are rarely reported.⁴¹

Heterogeneity in the design of MOFs can also be achieved by integrating two or more non-identical organic linkers with similar or multiple coordination groups, whether being homotopic, heterotopic or both, with the goal of producing a single extended hybrid structure.⁴² Nearly all examples of hetero-MOFs reported are synthesized from two linkers, each having a different coordinating group, originally carboxylates mixed with bipyridines or pyrazines. However, the generation of SBUs and the directionality of the structure is mainly served by the carboxylate linkers. Nevertheless, the incorporation of two or more linkers together often fails either due to its segregation

into separate phases to form two different MOFs or due to the incorporation of only one linker without the other. In contrast, upon the combination of ditopic and tritopic linkers, the synthesis of such complex topologies was reported in 2008.

As it can be seen in **Figure 1.7**, UMCM-1 $[(Zn_4O(COO)_6)_3(BDC)_4(BTB)_4]$ (BDC = 1,4-benzenedicarboxylate, BTB = 4,4',4''-benzene-1,3,5-triyl-tribenzoate) is one example of incorporating ditopic and tritopic linkers to form a highly porous and open MOF structure. Upon extending the lengths of the ditopic and tritopic linkers, an even more porous framework, such as MOF-210 $[(Zn_4O(COO)_6)_3(BPDC)_3(BTE)_4]$ (BPDC= Biphenyl-4,4'-dicarboxylate, BTE = 4,4',4''-(benzene-1,3,5-triyl-tris(ethyne-2,1-diyl))tribenzoate), was obtained. Additionally, MOFs integrating three different carboxylate linkers, containing a tritopic linker and two ditopic linkers of different lengths, has also been reported such as UMCM-12 $[(Zn_4O(COO)_6)_2(TPA)_2(BDC)(TMTPDC)_2]$ (TPA = 4,4',4''-nitriлотriбензоате, BDC= 1,4-benzene dicarboxylate, TMTPDC = 2',3',5',6'-tertramethylterphenyl-4,4''- dicarboxylate). Such materials have been shown to have some of the highest surface areas and pore volumes reported, which highlights the advantageous mixed linker strategy used in synthesizing MOFs.⁴³

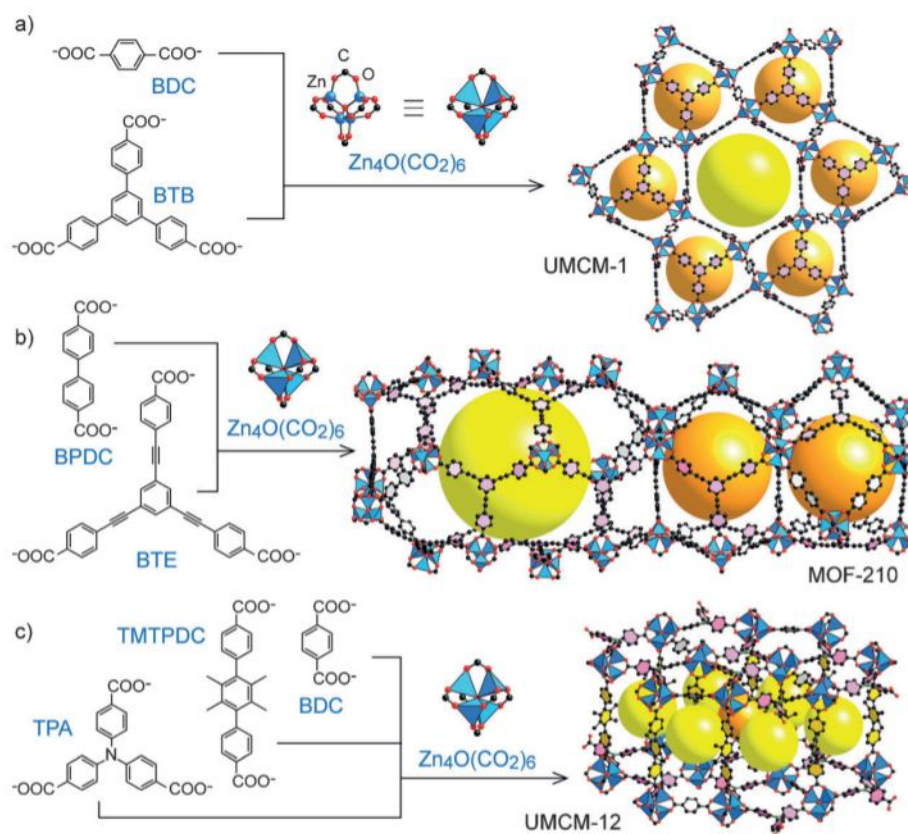


Figure 1.7. Crystal structures of (a) UMCM-1 (b) MOF-210 and (c) UMCM-12 which are composed of di- and tri-topic linkers connected to a $\text{Zn}_4\text{O}(\text{COO})_6$ SBU. $\text{Zn}_4\text{O}(\text{COO})_6$ (blue polyhedron); Oxygen (red); Carbon (black). The large yellow and orange spheres represent the different voids occupying the cavities of MOFs⁴³

3. Heterogeneity in heterotopic linkers

Expanding the scope of organic ligand coordination to integrate multiple heterotopic linkers within the MOF's structure is still a challenge; due to the uncertain coordination of the metal centers to all the functionalized ligand types. However, due to the presence of two or more coordinating sites in heterotopic linkers, one coordinating unit directs the formation of structure, porosity, flexibility or rigidity, directional binding and SBUs predetermination; while other types of coordinating units complement functional properties which include conductivity, chemical or thermal stability, nature of porosity (hydrophilic/hydrophobic), susceptibility for post-modification or availability of open metal sites.⁴⁴⁻⁴⁶ Moreover, bearing various binding groups, such linkers may favour the

formation of different types of SBUs within the same MOF framework.⁴⁷ For instance, in 2017, Tu et. al reported the formation of two MOFs coordinating H₂PyC = 4-pyrazolecarboxylic acid as linker with unprecedented topologies, namely FDM-4 and FDM-5.⁴⁸ In FDM-4, the first trinuclear SBU is formed via the coordination of Cu(II) ions with the pyrazolate end of the linker, while the Zn(II) ions coordinate octahedrally with all the carboxylate ends and partially via additional pyrazolates causing different variations within the Zn₄O(COO)₆ cluster (**Fig. 1.8**). Moreover, FDM-5 demonstrates, in addition to triangular Cu(II) SBU, triangular Zn₂(COO)₃ and trigonal-bipyramidal Zn₂(COO)₄(NN) clusters. Despite the short linker used, such MOFs feature micropores and mesopores with Brunauer–Emmett–Teller (BET) surface areas as high as 3728 m².g⁻¹.

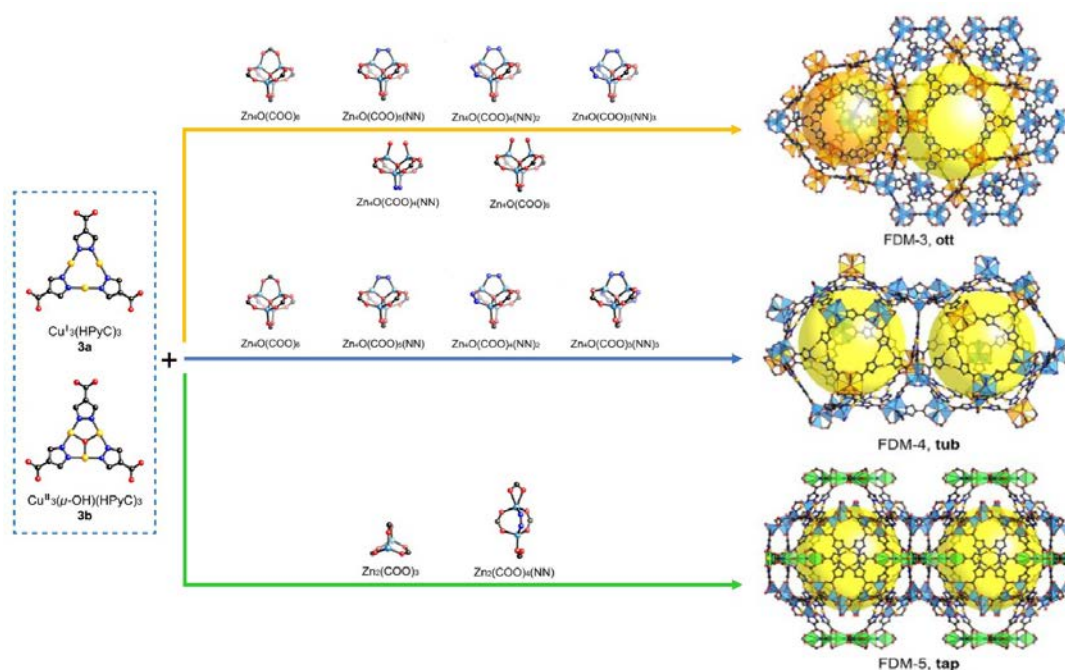


Figure 1.8 Incorporation of heterotopic linker (H₂PyC = 4-pyrazolecarboxylic acid) yields different SBUs producing multi-component MOFs of different topologies. Copper (yellow); Zinc (aqua), Nitrogen (blue), Oxygen (red); Carbon (black). The large yellow and orange spheres represent the different voids occupying the cavities of MOFs.

4. *Multivariate metal–organic frameworks*

Another scenario in the design of heterogenous MOFs may arise upon the introduction of two different functionalized linkers having the same backbone but are chemically distinct, or multiple metal ions forming the same type of SBU, to achieve further heterogeneity in frameworks known as multivariate (MTV) MOFs.⁴⁹ Interestingly, such defects incorporated to form MTV-MOFs exhibit the same overall topology as the parent framework; however, with additional properties or functionalities.

i. Multi-Metal MTV-MOF

The first multivariate MOF to be reported having a variety of BDC derivatives is MTV-MOF-5.⁵⁰ The implementation of a mixture of BDC linkers having different functional groups, BDC-X where X = -H, -NH₂, -Br, -(Cl)₂, -NO₂, -(CH₃)₂, -C₄H₄, -(OC₃H₅)₂, and -(OC₇H₇)₂, resulted in the synthesis of a single MOF containing up to 8 distinct functionalities in one phase, rather than mixed phases (**Figure 1.9**). The strategy of assembling different functional groups covalently linked to the same organic link (BDC), whose length and connectivity is unchanged, results in multivariate isostructural MOF, similar in crystallinity, topology and porosity of MOF-5. Intriguingly, an enhancement in CO₂ uptake capacity up to 400 % in MTV-MOF-5 in contrast to MOF-5 was observed due to an increased number of adsorption sites present in the pores of the multivariate system.

ii. Multi-Metal MTV-MOFs

In contrast to MTV-MOFs containing multiple organic linkers with different functionalities, the introduction of various metals within the same coordination

environment of SBUs is another extensive approach to achieve heterogeneity within MOF structures. The latter is either achieved via one-pot reaction synthesis or via post-synthetic metal exchange reactions. Co-doped MOF-5 have been recently reported by which 8% of the Zn incorporated SBUs have been exchanged with Co respectively.⁵¹ Nonetheless, detailed examination of the structure analysis reveal that the precise location of these doped Cobalt ions is still not clear. Additionally, a more recent work explores the incorporation of 10 different kinds of divalent metal ions including Mg, Ca, Sr, Ba, Mn, Fe, Co, Ni, Zn, and Cd into the same SBU of MOF-74 [$Zn_2(DOT)$] (DOT= dioxidoterephthalate) framework in a one-pot reaction synthesis (**Fig. 1.9**).⁵²⁻⁵³ This approach allows the distribution of metal ions to be incorporated within a single SBU resulting in a single phase MOF. Although the spatial distribution of these metal ions is not uniform, it is an advantageous method in heterogeneity as these ions could not be employed individually in the synthesis of pure phase MOFs. The developed mixed metal systems demonstrated an enhancement in the MOF's gas adsorption performance, in addition to improved catalytic activities.

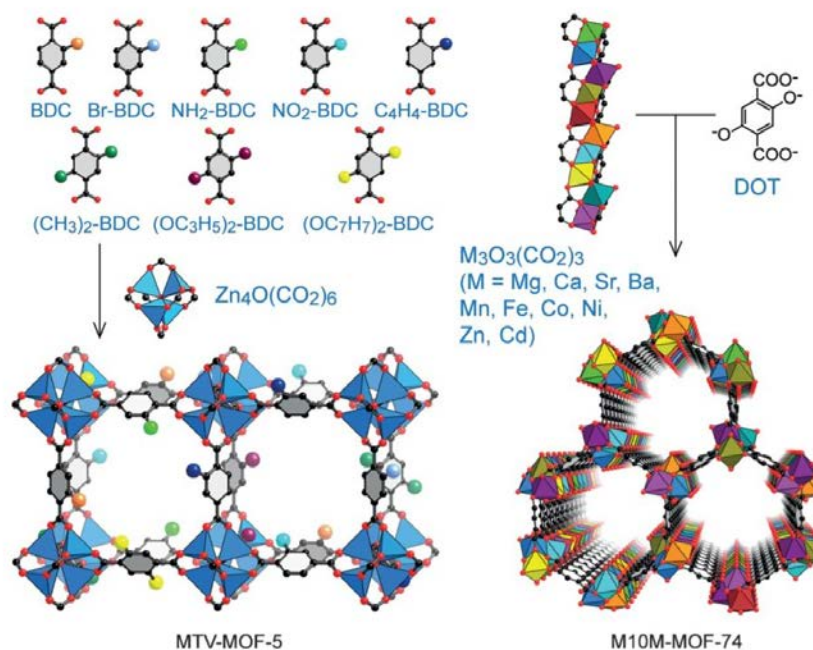


Figure 1.9 MTV-MOF-5 with various functionalized organic linkers incorporated within the same structure (left), MTV-MOF-74 of different metal ions SBUs (right)⁴³

D. Luminescent metal–organic frameworks

The development of metal–organic frameworks and the presence of a vast library of organic links and SBUs allows the tunability and structure diversity of various framework structures, which provides an advantageous contribution in a wide array of applications including gas storage, drug delivery, adsorption/extraction, catalysis and chemical sensing.⁵⁴⁻⁶⁰ Among these various applications, luminescent MOFs have attracted remarkable attention in recent years due to their low cost, high sensitivity, materials stability, reusability and short response time to guest molecules.⁶¹ This is mainly due to the ability of MOFs to entrap guest molecules of interest within their pores and keep them in close proximity to its luminescent centers, resulting in accumulated concentration of analytes, which act to either enhance (increase light emission), quench (decrease light emission) or exhibit a ratiometric (change in intensity

ratio at two different wavelengths) luminescence depending on its interaction with the inorganic centers and coordination compounds.⁶²⁻⁶³ Adding to that, many external factors are of interest with regards to changes in the photoluminescent intensity which include the introduction of particular guest molecules, temperature, pH and even humidity.⁶⁴⁻⁶⁸ Subsequently, the potential selectivity of different classes of analytes based on the MOF's apertures is yet important, wherein molecules smaller than the MOF's porous channels are absorbed, excluding larger molecules.⁶⁹ Such concept based on size exclusion, also known as molecular sieving, is directly controlled via the design of topology, nodes and organic links of MOFs; however, to date these systems have not been highly developed. Hence, the pore sizes and topologies of MOFs in addition to the presence of different exposed functional sites such as $-\text{NH}_2$, $-\text{OH}$, and pyridine sites act to enhance the MOF's ability to recognize different metal ions.⁷⁰⁻⁷¹ Although the weak intermolecular forces present between the organic linkers undoubtedly play a role in inducing luminescence functionality, the inorganic and organic moieties of the MOFs provide a more powerful role to provide luminescence through metal-to-ligand charge transfer (MLCT) or ligand-to-metal charge transfer (LMCT).⁷²⁻⁷³ Nevertheless, due to the variety of mechanisms proposed, the exact route involving guest-host interactions, electron charge transfer, or ionic vibrational processes remains a challenge. To this end, the hybrid nature of MOFs, enables a wide range of proposed emissive modes which act to generate luminescence as illustrated in **Figure 1.10**, which include:

1. Linker-based emission

Linker-based luminescence is common due to the typically conjugated ligands incorporated within the MOF's framework, especially with largely electronically inert d^{10} metal ions such as Zn(II) and Cd(II), that absorb in the visible or ultraviolet

spectrum. Emission may correspond to be directly emitted from the linker, or due to the involvement of charge transfer with the coordinated metal ions/clusters. Another approach reported to achieve luminescent MOFs is interlocking rather non-emissive linkers into the framework of MOFs in order to activate and enhance the luminescence properties of such linkers. Recently, the photostability of porphyrin has shown a remarkable enhancement upon locking it in a Zr-based MOF-525.⁷⁴⁻⁷⁵ Additionally, the introduction of functionalized organic linkers into MOFs structures is demonstrated by ligand exchange or post synthetic modification as another powerful tool to fabricate luminescent MOFs. For instance, emission maxima have been reported to change from borderline ultraviolet to visible emission upon the incorporation of 1,1,2,2-tetraphenylethylene in bio-MOF-101 upon irradiation with ultraviolet light.⁷⁶

2. Framework metal ions

Metal-centered emission is primarily seen in lanthanoid ions as nodes which comprise the f-block of the periodic table. Most transition metal elements containing unpaired electrons in their d-orbitals are often selected as efficient quenchers (electron acceptors), with the exception of d^{10} metal ion centers due to their unique configuration.⁷⁷ In contrast, lanthanoid ions are known to emit sharp yet weak luminescence as most suffer from weak light absorption and low quantum yields. Thus, in most cases, highly conjugated struts coordinated to the nodes of lanthanoid ions or the proximity of an organic fluorophore within the framework act as antennas to amplify the luminescence emission, wherein light is absorbed by the organic counterparts to later transfer to lanthanoid ions, hence generate luminescence. However, the method of tuning luminescent properties by the exchange of metal ions present in the nodes of MOFs have been also reported. One example relies in the

exchange of Zn(II) ions in $Zn_3L_2(DABCO)$ ($H_3L = [1,1':3',1''\text{-terphenyl}]$ -4,4'',5'-tricarboxylic acid and $DABCO = 1,4\text{-diazabicyclo}[2.2.2]\text{octane}$) with Cu(II) ions to obtain Zn_2Cu -MOF and $ZnCu_2$ -MOF.⁷⁸ Remarkably, these MOFs exhibit distinct photoluminescence properties, especially in contrast to Cu_3 -MOF which demonstrates non-emissive properties, where the incorporation of Zn(II) within the framework to obtain Cu_2Zn -MOF also demonstrates a strong emissive response.

3. Encapsulated luminophores

The presence of pores in MOFs provides a powerful platform to entrap fluorophores and other luminescent molecules to induce emission in an otherwise non-emissive MOF. Alterations in the design of MOFs by tuning their hydrophilicity/ hydrophobicity, polarizability, size or chemical structure (functional groups) increase the control and selectivity of the sensing analytes.⁷⁹ Previous work have reported the enhancement of photoluminescence by the introduction of aromatic guest species, where the quantum yield was proven to increase upon the absorption of benzene and toluene, in contrast to the empty framework where minimal luminescence was observed.⁸⁰⁻⁸¹ Furthermore, the in-situ encapsulation of fluorophores to generate white light from a blue light source have been reported by Jing Li et. al.⁸² It has been shown that using ZIF-8 and UiO-66 frameworks to encapsulate yellow dye molecules as a host-guest composites, emit white light that is initially excited by blue light with an increased quantum yield, making it compatible with the recent commercial LED technology by simple coating of LED lamp.

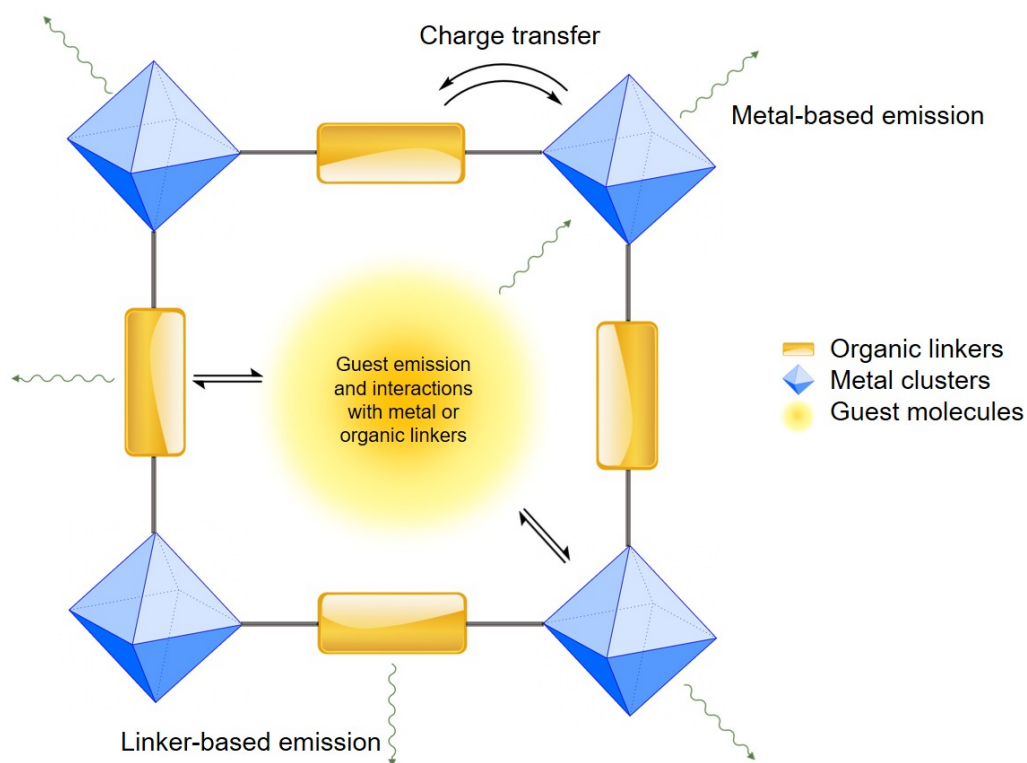


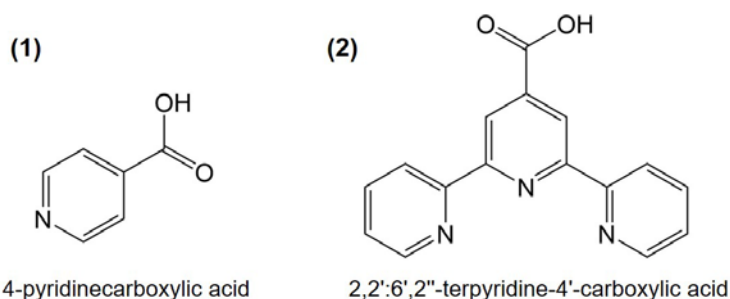
Figure 1.10 Scheme depicting emission possibilities in a MOF structure

Consequently, potential signal transduction from luminescent MOFs adopt several mechanisms. One of which is the solvchromatic effect, by which a wavelength shift in the absorption band, thus in luminescence emission spectra is observed upon change in in polarity of solvent.⁸³ Nonetheless, knowing that MOFs are robust and do not dissolve in common solvents, the effect is observed in the solid-state where the dispersion of crystals in solvents of different polarities results in a change in polarity of the absorbed guest molecules within the pores of MOFs, indicating the magnitude of solvent-MOF interactions. Secondly, alteration of the electronic structure via changes in the coordination spheres of MOFs affects the luminescence spectrum substantially. For instance, having large coordination spheres (coordination numbers up to 12 are known), Ln(III) ions present as nodes in MOFs have the ability to bind and interact with guest molecules directly, while being coordinated to the framework, to either increase or

decrease the luminescence intensity.⁸⁴ The third is the most common form of signal transduction which is photo-induced by absorption of guest molecules resulting in quenching (turn-off), enhancement (turn-on) or occasionally a ratiometric probe. The nature of these guest molecules indicates the relevant interactions with the structure framework, whether they are electron donors or acceptors, thereby inhibiting or enhancing the emitted signal.⁸⁵⁻⁸⁶ Nonetheless, several drawbacks result in the latter detection in luminescent MOFs, due to the effect of analyte concentration, coordination environment and excitation wavelength, which results in low accuracy recognition.⁸⁷ Therefore, ratiometric sensing probes act to eliminate such shortcomings of a single fluorescent signal by being independent of the above interfering factors; due to the presence of multiple, self-calibrated and dual emission intensity signals that achieve increased levels of detection.⁸⁸ This technique is commonly accompanied by colorimetric changes as it mainly relies on the changes of the intensity of two or more emission peaks that are induced by specific analytes, which in return provides an internal standard and self-reference that results in a more accurate and sensitive detection of analytes, disregarding any external interference from the environment. Lastly, formation of an exciplex is yet another signal transduction mechanism where π - π interactions between adjacent conjugated organic linkers or between an absorbed guest molecule with a framework strut produces an excited complex upon absorption of a photon, resulting in a unique and broad emission band. The orientation of the component molecules, in addition to their separation distance is significant in this emission state.

OBJECTIVES

This thesis outlines a strategy for making novel MOFs from heterotopic linkers to enhance and develop its performance in luminescent sensing applications. Such a construct can be achieved by using linkers that have two or more different chelating functionalities, in order to prepare a set of new materials with unprecedented chemical, topological and photophysical properties, which will be explored for various applications, mainly chemical sensing. In this thesis, the first primary focus is based on 4-pyridinecarboxylic acid linker (**1**) which incorporates carboxylate and pyridine coordination sites. Secondly, another focus relies on integrating a more complex heterotopic linker such as 2,2':6',2''-terpyridine-4'-carboxylic acid (cterpy) (**2**) which incorporates three pyridine and one carboxylate coordination sites. The use of such linkers resulted in the formation of two new MOFs having Cu(II) as a metal center, which are mainly employed to explore the concept of heterogeneity within order and its various applications in chemical sensing.



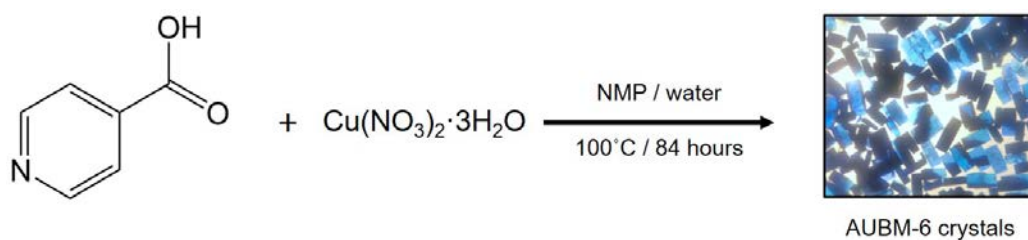
CHAPTER II

MATERIALS AND METHODS

All reagents and chemicals were commercially available from Sigma-Aldrich and used without any further purification.

A. Synthesis of AUBM-6

$\text{Cu}(\text{NO}_3)_2 \cdot 3\text{H}_2\text{O}$ (0.4095 mmol, 98.94 mg) and isonicotinic acid (INA, 0.0819 mmol, 10 mg) were dissolved in a mixture of 2 mL N-methyl-2-pyrrolidone (NMP) and 1 mL deionized water in a 4 mL vial. After being sonicated for 10 min, the subsequent solution was heated at 100 °C for 84 hours. The resulting blue single crystals (**Scheme 2.1**) were left to cool down at room temperature then washed three times with NMP and three times with methanol to obtain 83% yield based on INA. The fabrication of AUBM-6 nanosheets (AUBM-6-NS) was done via top-down liquid ultrasonication exfoliation method, by which 10 mg of the crystals were placed in 10 mL acetonitrile and ultrasonicated for 10 hours at room temperature. A blue colloidal suspension was obtained and centrifuged at 10 000 rpm for 1 hour to get the AUBM-6-NS nanosheet materials.



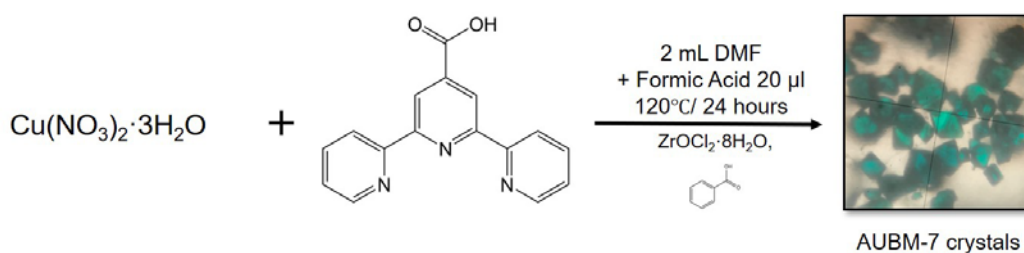
Scheme 2.1 Synthesis route of AUBM-6 crystals starting from INA ligand.

B. Synthesis of 2,2':6',2''-terpyridine-4'-carboxylic acid (cterpy) ligand

This compound is not commercially available and was provided by Dr. Tarek Ghaddar's research group. A mixture of 4-(2-furyl)-2,2':6',2''-terpyridine (0.2991 g, 1 mmol) and KMnO₄ (2.0544 g, 13 mmol) was added to 1:1 ratio THF/H₂O and stirred at room temperature for 24 hours. Then the suspension was filtered and washed with water and ethanol then recrystallized from DMF to give 2,2':6',2''-terpyridine-4'-carboxylic acid. All physical and spectroscopic properties were identical to previously reported data for this compound.⁸⁹

C. Synthesis of AUBM-7

ZrOCl₂·8H₂O (0.139 mmol, 25 mg) and benzoic acid (4.09 mmol, 0.5 g) were initially dissolved in 2 mL N-dimethylformamide (DMF) and heated at 100 °C for 1 hour. After the solution was removed and left to cool down at room temperature, Cu(NO₃)₂·3H₂O (0.028 mmol, 7 mg), 2,2':6',2''-terpyridine-4'-carboxylic acid (cterpy) (0.036 mmol, 10 mg) and 20 μl of formic acid were added to the solution and sonicated for 10 min then placed in the oven at 120 °C for 24 hours. The resulting green octahedral shaped crystals (**Scheme 2.2**) were left to cool down at room temperature then washed with DMF 3 times followed by acetone for 3 times to obtain 93% percentage yield based on cterpy linker.



Scheme 2.2 Synthesis route of AUBM-7 crystals starting from cterpy ligand.

D. FT-IR measurements

The Infrared (IR) spectra were recorded on a FT-IR spectrometer Thermo-Nicolet working in the transmittance mode, in the 450-3950 cm^{-1} range.

E. Thermogravimetric analysis

Thermogravimetric Analysis (TGA) was performed with Netzsch TG 209 F1 Libra apparatus within the ranges of 30°C and 1000°C.

F. Single Crystal X-ray Diffraction

Single crystal X-ray data were collected using Bruker Kappa APEX II diffractometer with Mo-K α ($\lambda = 0.71073 \text{ \AA}$), the data were corrected for Lorentz and polarisation and a multi-scan absorption correction was applied using the APEX III suite. The structure was solved using the direct method and refined using least square method incorporated in SHELXTL package. Since the AUBM-6 crystals were twinned due to the stacking of the plates, one phenyl ring was partially disordered while the solvent molecules were completely disordered.

G. Powder X-ray Diffraction

Powder X-ray diffraction (PXRD) patterns were collected using a Bruker D8 advance X-ray diffractometer (Bruker AXS GmbH, Karlsruhe, Germany) at 40 kV, 40 mA (1600 W) using Cu-K α radiation ($\lambda = 1.5418 \text{ \AA}$). The PXRD patterns were collected via 2θ from 5° to 50° and a step size of 0.01° overnight.

H. Scanning Electron Microscopy

Scanning electron microscopy (SEM) was performed using a MIRA3 Tescan electron microscope, where the samples were first coated with a thin layer of platinum at an acceleration voltage of 5-15 kV.

I. Brunauer–Emmett–Teller (BET) surface area measurement

The Brunauer–Emmett–Teller (BET) surface area was measured using a Quantachrome-NOVA 2200e-Surface Area and pore size analyser. The sample crystals were degassed under Nitrogen at a temperature of 150 °C for 12 hours.

J. UV-Vis spectroscopy

The absorption spectra were recorded at room temperature using JASCOV-570 UV-vis-NIR spectrophotometer. The sample crystals were initially dispersed in acetonitrile and UV-Vis measurement was performed.

K. Fluorescence spectroscopy

The steady state fluorescence measurements were recorded with resolution increment of 1 nm, slit 5 using a HORIBA Jobin Yvon Fluorolog-3. The excitation source was 100 W xenon lamp, and the detector used was an R-928 operating at a voltage of 950V. To regulate the temperature, a thermostat was coupled with the sample holder.

L. Solvent titrations

Suspensions of AUBM-6-NS were initially prepared by dispersing 5.00 mg in 10 mL acetonitrile (CH₃CN) solution for 10 min. Microvolumes (10 to 1000 μl) of 2% by volume of acetone, chloroform, dichloromethane (DCM), dimethylformamide (DMF), dimethylacetamide (DMA), tetrahydrofuran (THF), N-methyl-2-pyrrolidone (NMP), methanol, 1-butanol and 2-propanol in addition to pure deionized water were gradually sensed against 3 mL standard emulsion of AUBM-6-NS. Intensity enhancement and a bathochromic shift demonstrating a ratiometric probe was only observed for acetone.

M. Metal ions titrations

The nitrate metal salts used for luminescence sensing at room temperature are Mⁿ⁺ : [Fe³⁺, Fe²⁺, Al³⁺, As³⁺, Mg²⁺, Co²⁺, Cd²⁺, Ni²⁺, Cu²⁺, Cu⁺, Mn²⁺, Hg²⁺, Zn²⁺, Cr³⁺, Ca²⁺, Pd²⁺ and Ag⁺]. AUBM-6 (5.00 mg) and AUBM-6-NS (5.00 mg) were dispersed and ultrasonicated separately in 10 mL acetone for 10 min where the colloidal suspension was obtained for each. The sensing measurements of 3 mL standard emulsions of AUBM-6 and AUBM-6-NS were performed by adding gradual volumes of the metal cation solutions having 2.5 ppm initial concentrations. Each titration measurement was performed twice for reproducibility. No shift in the main absorbance band of the MOF was observed; however, only intensity quenching was noted in the emission spectra during titrations.

CHAPTER III

SYNTHESIS, CHARACTERIZATION AND APPLICATION OF TWO-DIMENSIONAL METAL–ORGANIC FRAMEWORK AUBM-6

A. Introduction

The synthesis of metal–organic frameworks, with various porous voids that are self-assembled from metal ions/cluster and multitopic organic linkers have attracted considerable amount of interest during the past decade, due to their promising applications in gas storage/separation, sensing, molecular sieving and catalysis.⁹⁰⁻⁹⁵ Current research on MOF luminescent sensing probes focus on the design of 3-dimensional bulk-sized MOFs that in return limits their up-close interactions with targeted metal ions.⁹⁶⁻⁹⁷ In order to synthesize an effective MOF sensor, binding sites, powerful luminophore and a stable morphology are needed. Adding to that, using π -conjugated organic molecules also play a significant role in providing adequate binding sites for different metal ions.⁹⁸⁻¹⁰⁰ For instance, 4-pyridinecarboxylic acid, also known as isonicotinic acid (INA), having a whole π -conjugated backbone, tends to afford π - π interactions either between adjacent conjugated ligands or adjacent guest molecules upon its incorporation within the MOF's framework.

It is still a great challenge to obtain 2D MOFs with atomic or molecular thickness in high yields; nevertheless, previous methods have reported the exfoliation of 3D layered MOFs into their complementary 2D nanosheets, hence retaining their structure and topology.¹⁰¹⁻¹⁰³ Such exfoliation process is mainly based on delaminating these

frameworks that are held together by weak interactions including van der Waals or hydrogen bonding. Moreover, having relatively increased surface areas and ultrathin thickness, the exfoliated 2D nanosheets exhibit more accessible active sites.¹⁰⁴ As a result, the complementary luminescent sensing properties either increase in sensitivity, rate, activity or efficiency.

The development of sensitive and selective luminescent diagnostics towards late and heavy transition metals is of immense and elevating interest, due to their various cytotoxic effects and environmental and health complexities.¹⁰⁵ On one hand, a rare transition metal, palladium (Pd^{2+}), is known to have a wide spectrum of hazardous health effects even in minimal concentrations, which include skin and eye allergies, perturbations of cellular processes and various environmental hazards.¹⁰⁶⁻¹⁰⁷ For instance, previous investigations have indicated that Pd^{2+} ions can bind to DNA, proteins, or other macromolecules such as vitamin B6¹⁰⁸. Apart from this, it is well established that several environmental agencies restrict the maximum dietary intake of palladium to less than 1.5 -15 μg per day per person; in addition to its threshold in drugs to be 5-10 ppm¹⁰⁹⁻¹¹⁰.

On the other hand, acetone, being a common solvent that plays a vital role in the chemical industry, is known to be volatile, by which it irritates the eyes, skin and respiratory tract upon too much exposure¹¹¹. Recently, luminescent MOFs have attracted remarkable attention due to their advantageous ability to entrap guest molecules of interest within their pores and keep them in close proximity to their active centers¹¹². To date, there exist several MOFs previously reported for acetone sensing; however, most of these MOFs exhibit lanthanide based-metal centres and only a few transition-metal centres demonstrate unique selectivity towards detection of acetone molecule.¹¹³⁻¹¹⁴ It is worthy to note that most of the latter reported MOFs exhibit a “turn-off” luminescent

sensor; none of which exhibit a ratiometric characteristic probe. Up until recently, ratiometric detection has taken a high toll in being successful methods in addressing hybrid systems or organic fluorophores.¹¹⁵

In this chapter, we report the synthesis and characterization of a chemically stable (in common solvents) 2D-layered MOF, namely AUBM-6 (AUBM= American University of Beirut Materials) and the fabrication of its layered structure into its complementary 2D thin nanosheets via top-down liquid ultrasonication exfoliation method. While the copper-based MOF was investigated for photo-luminescence (PL) sensing towards different metal ions and solvents, it was concluded that AUBM-6 is selective towards Pd²⁺ and acetone specifically having a “turn-off” and ratiometric diagnostic probes respectively. To the best of our knowledge, there isn’t a reported transition metal-based MOF exhibiting a ratiometric mechanism towards acetone detection.

B. Results and Discussion

1. Description of Crystal Structure

AUBM-6 crystals feature a 2D rectangular prism shape with multi-layered structure topology as it can be seen in **Fig. 3.1**. Single-crystal X-ray diffraction analysis reveals that the compound crystallizes in the orthorhombic, non-centrosymmetric space group $Pca2_1$ with the lattice parameters of $a = 23.8349(6) \text{ \AA}$ $b = 5.80370(10) \text{ \AA}$ $c = 13.1873(3) \text{ \AA}$ and cell volume $1824.21(7) \text{ \AA}^3$ (**Table 3.1**). All the atoms are located at the general Wyckoff position 4a. The asymmetric unit cell contains one Cu(II) ion, two crystallographically independent INA ligands, one water molecule and one NMP solvent. The obtained formula of the structure is $C_{17}H_{17}CuN_3O_6$. In order to verify that the geometry of the penta-coordinated Cu(II) in the MOF structure is square pyramidal,

the structural parameter ($\tau_5 = \frac{\beta - \alpha}{60}$) is investigated by which its value was found to be 15.8 % where α (N-Cu-N) = 168.9° and β (O-Cu-O) = 178.5° represent the two basal angles. Hence, in ideal square pyramidal geometry, $\tau_5 = 0$ %, $\alpha = 180^\circ$ and $\beta = 180^\circ$ are reported.¹¹⁶⁻¹¹⁷ The obtained τ_5 demonstrates a very small deviation of 15.8 % due to the distortions in INA ligand. The Cu(II) ion is coordinated to 4 INA ligands bonded through alternating carboxylate and nitrogen ends to form one mononuclear heterotopic secondary building unit (SBU) and also connected to water oxygen with bond distances: Cu-O (carboxylate) around 1.94 Å, Cu-N 2.02 Å and 2.04 Å and Cu-O (water) around 2.24 Å. The coordination of water oxygen to Cu(II) center orients perpendicularly to the square planar INA ligands, forming the square pyramidal geometry; nevertheless, this oxygen was omitted for structure clarity purposes. The Cu-INA ligands are bridging through the N and O to form 2D-multi layers as shown in **Fig. 3.1**. The carboxylate and pyridine units attached to Cu(II) are in trans positions, hence two of the uncoordinated oxygen atoms point either towards or away from the subsequent layer. There exist one-dimensional porous channels centered around the distorted squared $\text{Cu}_4(\text{INA})_4$ units with the Cu-Cu distances of 8.85 Å and 8.93 Å and the Cu-Cu diagonal distances of 11.93 Å and 13.19 Å. The distance between these layers is the size of the b-axis and it is around 5.80 Å taking the Cu-ions as reference. The layers are weakly connected to each other through hydrogen bonds between water and nitrogen and carboxylate groups. These interactions present between the layers are critical for delamination to occur by ultrasonic exfoliation.

Table 3.1 Crystal data and structure refinement of AUBM-6**AUBM-6**

Empirical formula	C ₁₇ H ₁₇ CuN ₃ O ₆
Formula weight	413.80
Temperature, K	296(2)
Wavelength, Å	0.71073
Crystal system	Orthorhombic
Space group	Pca2 ₁
a, Å	23.8349(6)
b, Å	5.80370(10)
c, Å	13.1873(3)
α, deg	90°
β, deg	90°
γ, deg	90°
Volume, Å ³	1824.21(7)
Z	4
Density (calculated), Mg/m ³	1.507
Absorption coefficient, mm ⁻¹	1.235
F(000)	832
Crystal size, mm ³	0.150 x 0.150 x 0.150
Theta range for data collection	3.419 to 25.997°.
Index ranges	-25 ≤ h ≤ 29, -7 ≤ k ≤ 6, -16 ≤ l ≤ 15
Reflections collected	9627
Independent reflections	3523 [R(int) = 0.0369]
Completeness to theta = 25.242°	99.7%
Absorption correction	Semi-empirical from equivalents
Max./min. transmission	0.7460 and 0.7111
Refinement method	Full-matrix least-squares on F ²

Data / restraints / parameters	3523 / 31 / 235
Goodness-of-fit on F^2	1.371
Final R indices [$I > 2\sigma(I)$]	$R_1 = 0.0540$, $wR_2 = 0.1364$
R indices (all data)	$R_1 = 0.0573$, $wR_2 = 0.1380$
Absolute structure parameter	0.099(11)
Extinction coefficient	N/A
Largest diff. peak and hole $e\text{\AA}^{-3}$	0.869 and -0.620

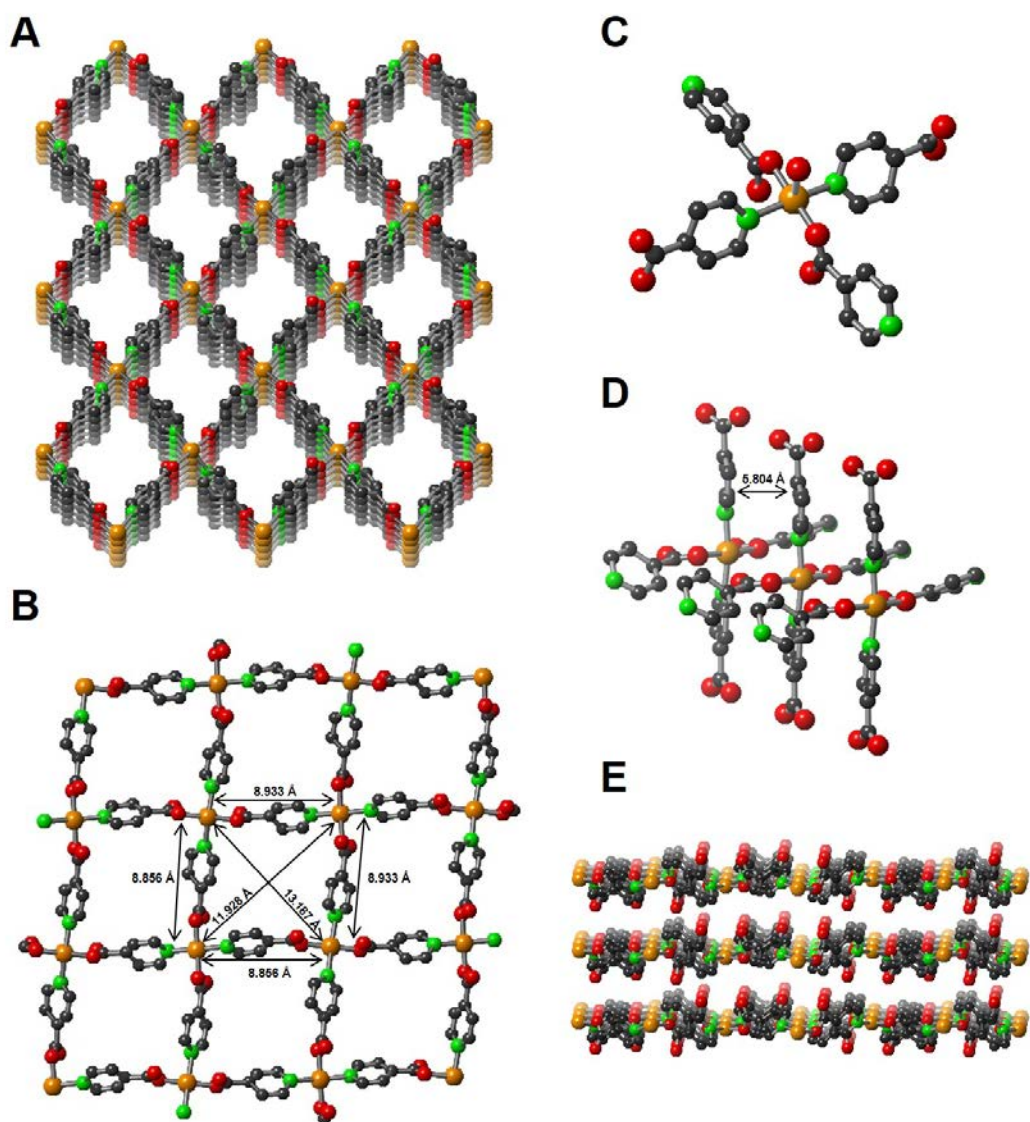


Figure 3.1 (A) Multi-layer view of the 1D channels of AUBM-6 ($\text{C}_{17}\text{H}_{17}\text{CuN}_3\text{O}_6$). (B) Coordination mode dimensions of AUBM-6. (C) Coordination environment of the Cu^{2+} ion in AUBM-6. (D)(E) 2D multi-layer side view of AUBM-6. Copper (gold); Oxygen (red); Nitrogen (green), Carbon (black).

2. PXRD Patterns and Thermogravimetric Analysis

The phase purity of the synthesized 2D AUBM-6 and AUBM-6-NS was verified by PXRD by comparing the simulated and experimental patterns. The experimental diffraction peaks are shown to be in good agreement with the simulated one as shown in **Fig. 3.2.A** This verifies the crystalline identity and the purity of AUBM-6 and AUBM-6-NS samples. The thermostability of AUBM-6 was studied by thermogravimetric analysis (TGA) (**Fig. 3.2.B**) at the temperature range of 30-700°C. The TGA curve represented a two-steps weight degradation within this temperature range. The first step is demonstrated from 30 to 100 °C with an estimate of 3.71% weight loss attributed to the escape of water molecules from the framework. The second 53.13% weight loss is represented by a steep decline at 250 °C establishing a correlation with the decomposition of the MOF structure and discharge of the organic ligands.

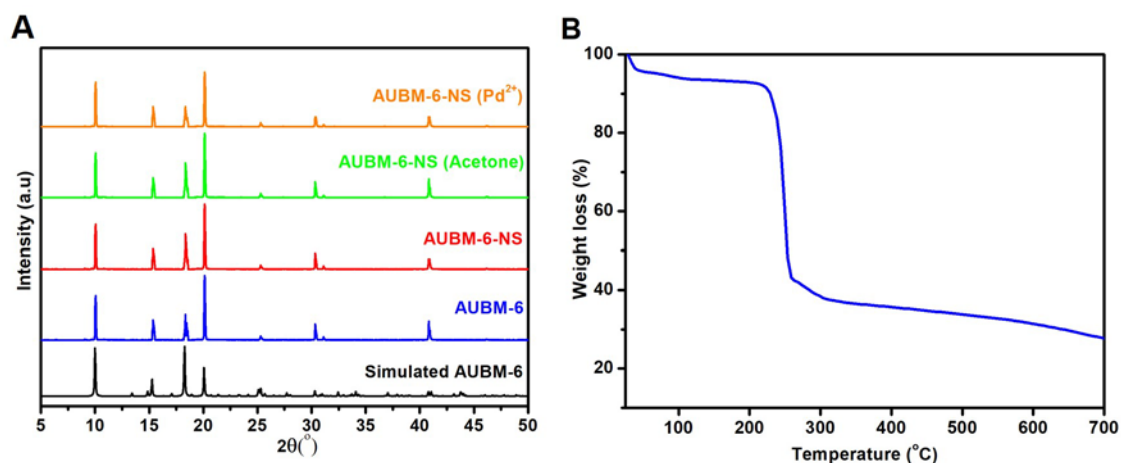


Figure 3.2 (A) Simulated and experimental PXRD patterns of AUBM-6 and AUBM-6-NS before and after acetone and Pd²⁺ sensing (B) Thermogravimetric analysis of AUBM-6

3. FT-IR spectrum analysis and BET surface area measurement

Analysis of the FT-IR spectrum of INA shows one weak band between 3000 cm⁻¹ and 3250 cm⁻¹ indicating the stretching vibrations of N-H secondary amine group (**Fig. 3.3**). The downfield shift of peaks at 1608.1 cm⁻¹ and 1384.6 cm⁻¹ in AUBM-6 towards

lower wavenumbers from the original peaks of INA present at 1409.7 cm^{-1} and 1712.5 cm^{-1} thus to lower energies favour the coordination of the metal cations to the organic linkers. The absence of the -OH stretching band at 2429.3 cm^{-1} in AUBM-6 verifies the carboxylate coordination group in INA to Cu^{2+} .

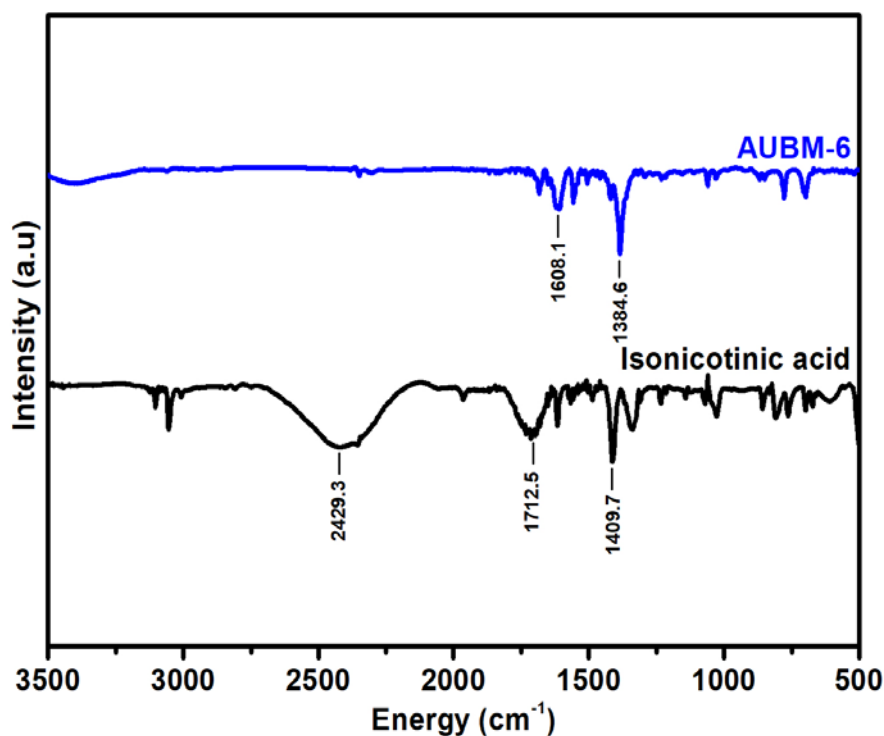


Figure 3.3 FT-IR spectrum of INA ligand and AUBM-6.

The N_2 sorption isotherm of AUBM-6 at 77 K shows a reversibility adsorption behaviour characterizing the layered microporous material (**Fig. 3.4**). BET surface area was calculated to be $233\text{ m}^2\cdot\text{g}^{-1}$.

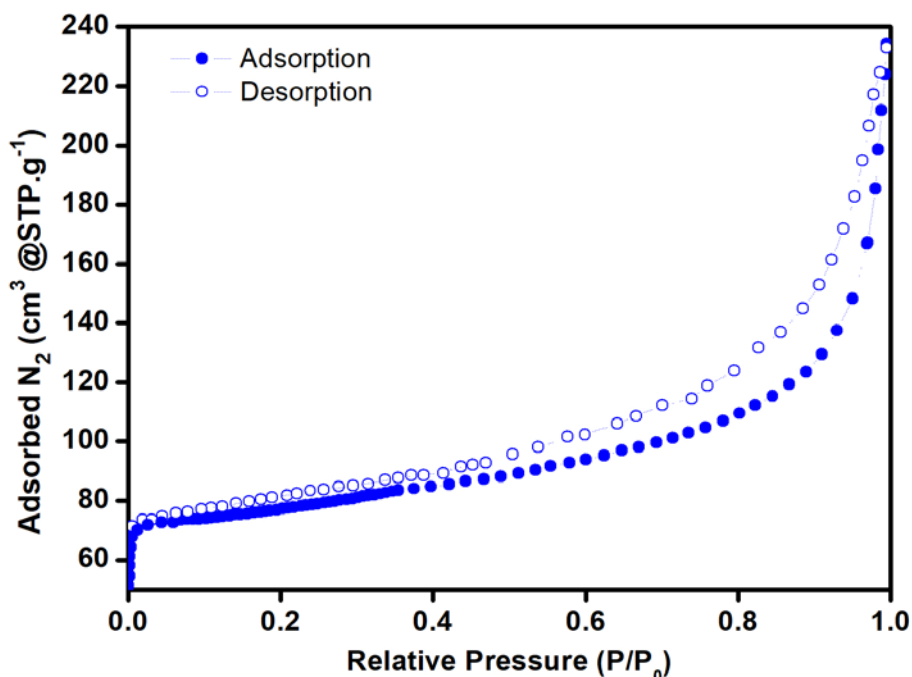


Figure 3.4 BET surface area measurement curve of AUBM-6.

4. Effect of exfoliation on PL-spectra of AUBM-6

The ultrasonic exfoliation of AUBM-6 resulted in few-layer nanosheets. To further confirm the delamination procedure, scanning electron microscopy (SEM) was carried out to investigate the morphologies of the exfoliated and non-exfoliated crystals. As shown in **Fig. 3.5**, SEM images of AUBM-6 reveal bulk rectangular crystals with a multi-layered structure having lateral dimensions up to 50 μm . In contrast, SEM images of the exfoliated AUBM-6-NS show a significant decrease in the lateral dimensions that varies to less than 200 nm. This demonstrates that the multi-layered structure of AUBM-6 withstands a strongly bonded intralayer assembly and exhibits weakly bonded interlayer interactions, which allow it to be readily delaminated into few-layer nanosheets, hence preserving its initial parent topology as evidenced by the PXRD pattern of the crystals performed after sonication (**Fig. 3.2.A**).

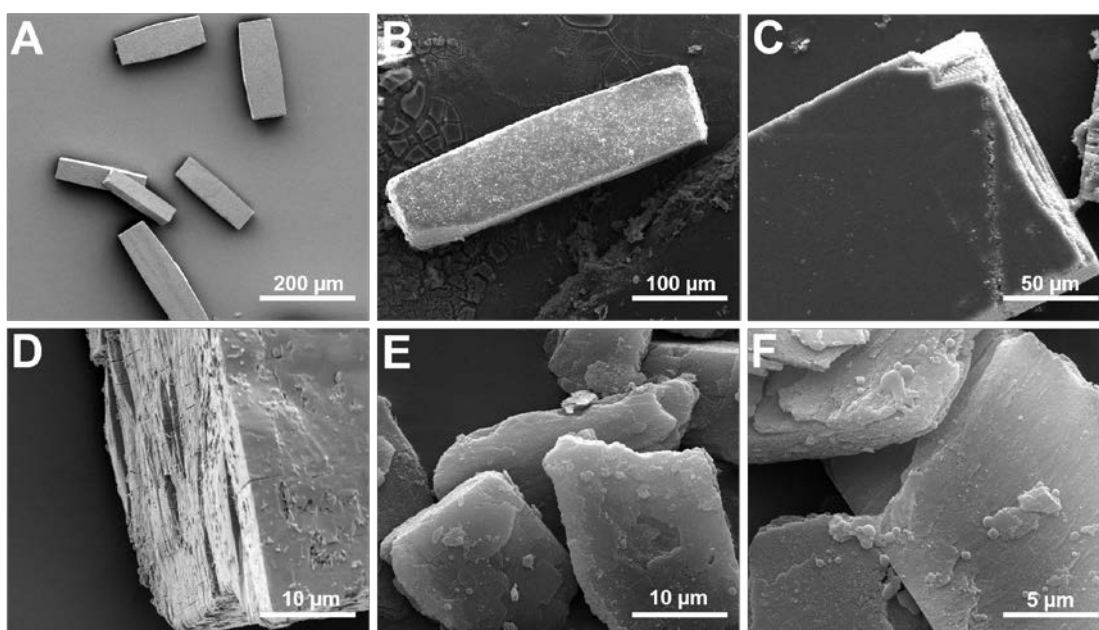


Figure 3.5 SEM images of (A) Bulk crystals of AUBM-6 (B) Single crystal of AUBM-6 (C)(D) Layered morphology of AUBM-6 (E)(F) Exfoliated few layer nanosheets of AUBM-6-NS

One reasonable explanation of the retention of topology between the 2D bulk and exfoliated materials is that ultrasonic waves generate shear forces or cavitation bubbles upon the layered species, generating high energies that result from the collapse of bubbles. Thus, such voids lead to break up the weak bonds between the layered species into their complementary single or multi-layered nanosheets without interfering in the intralayer structure of the MOF. The PL properties of the free INA ligand, AUBM-6 and AUBM-6-NS crystals were investigated at room temperature. As shown in **Fig. 3.6.A**, there is no overlap between the absorption spectrum of acetone and the excitation band of AUBM-6-NS, which confirms that acetone has no competitive energy absorption within the MOF's framework. As a result, this shows that acetone molecules may enhance ligand-to-metal charge transfer efficiency from INA ligand to Cu^{2+} centres.

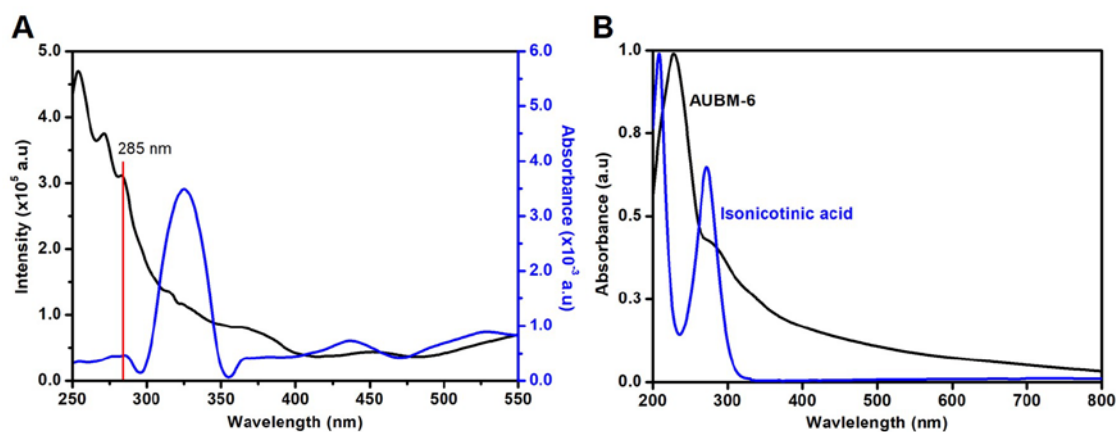


Figure 3.6 (A) UV adsorption spectrum of blank acetone (blue) and excitation spectrum of AUBM-6 (black) (B) UV-Vis Spectrum of INA ligand and AUBM-6 in acetonitrile CH_3CN .

Upon excitation at 285 nm (**Fig. 3.6.B**), AUBM-6 shows a broad emission peak at 409 nm, which may be attributed to π - π^* or n - π^* transitions (**Fig. 3.7**). Moreover, having the same emission band as INA, AUBM-6 is observed to have an induced ligand centred emission. It is noteworthy that the emission intensity of AUBM-6-NS is shown to be up to 3-folds greater than that of the bulk AUBM-6. Hence, it is proposed that the PL-spectra of the bulk AUBM-6 may exhibit a self-quenching mechanism, upon which their respective delamination into ultrathin nanosheets is observed to activate the MOF into its PL properties.

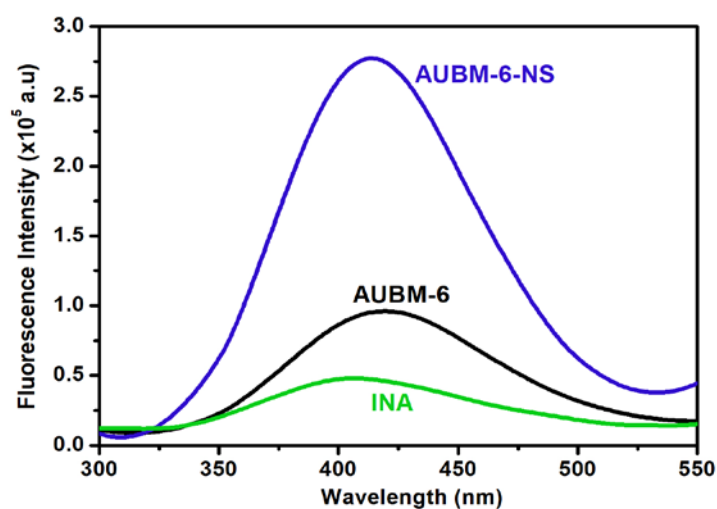


Figure 3.7 PL-spectra of INA, AUBM-6 and AUBM-6-NS in acetone at $\lambda_{\text{ex}} = 285 \text{ nm}$

5. *Ratiometric selectivity towards acetone*

AUBM-6-NS crystals were initially dispersed in acetonitrile CH_3CN solution at an excitation wavelength 285 nm. The PL-spectra gave a characteristic emission band at 317 nm as shown in **Fig. 3.8** Upon gradual titrations of different organic solvents, in addition to deionized water, the resultant peak emissions showed no significant change at 317 nm, except for acetone, where a red shift to 409 nm was observed. The most interesting feature is that upon the addition of increasing volumes of acetone, the luminescent intensity at 317 nm substantially decreased and a broad new emission peak at 409 nm gradually appeared. The addition of only 0.0067% of acetone initiates quenching of the initial parent intensity thus, the addition of 0.5% of acetone can completely quench the band centered at 317 nm (I_{317}) and generate a completely red shifted peak centered at 409 nm (I_{409}). Such a significant bathochromic shift not only enables the accurate sensing of acetone, but also induces an accurate measurement of the two emission intensities generated by a large ratiometric value variation. In fact, as the volume of acetone is increased, the emission intensity ratio (I_{409}/I_{317}) is found to be linearly proportional to the content of acetone added between the range of 0.0067-0.50%. The proposed mechanism behind the observed quenching effect of the parent peak may be attributed to minor interactions between the MOF's structure and acetone, by which upon excitation, energy is transferred from the INA ligands to acetone molecules resulting in a significant ratiometric effect. It is also suggested that the acetonitrile molecules that are weakly coordinated to the open metal sites of Cu^{2+} are gradually replaced by the acetone molecules, leading to their significant signal diminishing and peak shifting effects.

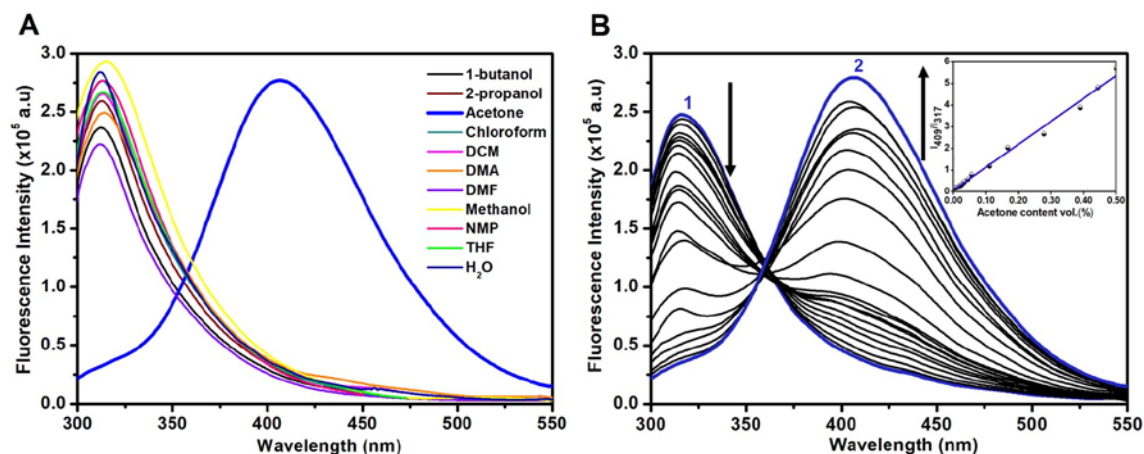


Figure 3.8 (A) PL-spectra of AUBM-6-NS upon addition of different organic solvents (2.0 vol%) at 1000 μl . (B) Ratiometric probe of AUBM-6-NS initially dispersed in CH_3CN upon gradual titration with acetone at (1) 0 μl and (2) 1000 μl . Inset: Intensity ratio at 409 nm and 317 nm PL emission of AUBM-6-NS upon addition of different amounts of acetone (at $\lambda_{\text{ex}} = 285 \text{ nm}$)

Unlike most lanthanide and transition metal-based MOFs that require pre-activation before performing the PL-spectra due to the hindrance effect of other solvent molecules present in their voids, the activation of AUBM-6-NS prior acetone detection is bypassed due to its ratiometric characteristic probe. Furthermore, as shown in **Table 3.2**, it is important to note that previously reported MOFs exhibit a “turn-off” mechanism towards acetone sensing, unlike AUBM-6-NS which interestingly demonstrates a ratiometric detection.

Table 3.2 Literature survey about previously reported MOFs towards acetone sensing. LOD: Limit of detection.

Luminescent Materials	Detection Method	LOD _{min} (vol%)	Ref.
Eu(BTC)(H ₂ O) _{2.5}	turn-off	0.31	[¹¹³]
Eu(BTB)(H ₂ O) ₂	turn-off	0.010	[¹¹¹]
Tb ₄ (μ ₆ -L) ₂ (μ-HCOO)(μ ₃ -OH) ₃ (μ ₃ -O)(DMF) ₂ (H ₂ O) ₄	turn-off	0.20	[¹¹⁴]
[Cd ₃ (tib) ₂ (BTB) ₂ (DEF) ₃] ₄ (H ₂ O) ₅	turn-off	0.075	[⁷⁷]
Cd ₃ (tib) ₂ (BTB) ₂ (DMA) ₂ (H ₂ O) ₂	turn-off	0.085	[⁷⁷]
Yb(BPT)(H ₂ O)(DMF) _{1.5} (H ₂ O) _{1.25}	turn-off	0.50	[¹¹⁸]
Tb(BTC)(H ₂ O) ₆	turn-off	0.28	[¹¹⁹]
Cd ₃ (L)(H ₂ O) ₂ (DMF) ₂ (DMF) ₅	turn-off	0.10	[¹²⁰]
Cd ₃ (dib)(L)](H ₂ O) ₃ (DMA) ₅	turn-off	0.20	[¹²⁰]
AUBM-6-NS	ratiometric	0.0067	This work

The PXRD pattern of AUBM-6-NS after acetone detection (**Fig. 3.2.A**) proves to be consistent with original sample, thus ruling out the collapse of the framework. The photostability of AUBM-6-NS in acetone was also examined as shown in **Fig. 3.9**. It is noteworthy that upon continuous excitation at 285 nm and collection of emission intensity at 409 nm for 60 min, only a 7% decrease in PL intensity was observed, hence it is believed that the dispersion of AUBM-6-NS in acetone is concluded to be stable and far from significantly inducing photodegradation.

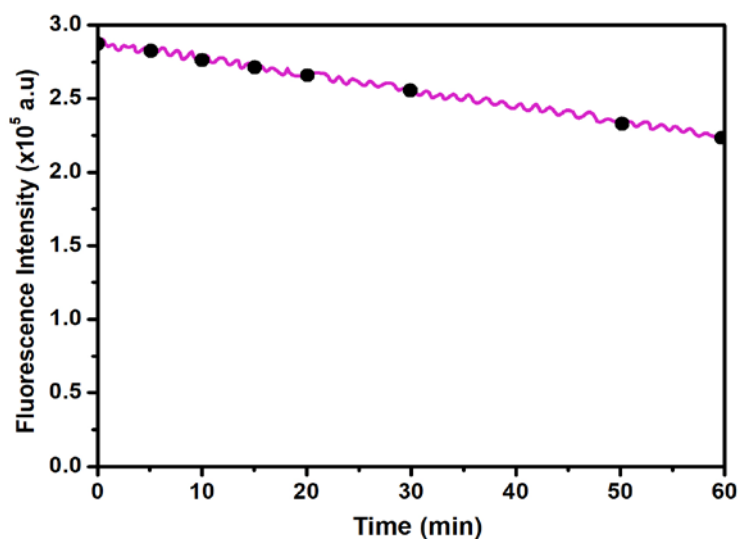


Figure 3.9 Fluorescence intensity versus time trajectories of AUBM-6-NS upon continuous excitation at $\lambda_{\text{ex}} = 285 \text{ nm}$

Moreover, the reversibility potential of the newly originated peak at 409 nm upon gradual increase in temperature was examined. Impressively, upon increasing the temperature from 25 °C to 30 °C, a noticeable decrease in I_{409} and an increase in I_{317} is observed as shown in **Fig. 3.10.A**. Upon further increase in temperature, a continuous decrease in I_{409} is noticed until $T = 50 \text{ °C}$, where a complete quenching resulted and a complete regeneration of I_{317} occurred. The gradual evaporation of acetone molecules resulted in the blue shift of intensity to its original parent peak (I_{317}), proving the AUMB-6-NS selectivity towards acetone. Moreover, to check the recyclability of the latter process, acetone was re-added, and the effect of temperature increase on the ratiometric process was studied. Remarkably, the regeneration of the peak at 317 nm and disappearance of the peak at 409 nm was achieved up to 5 times with no significant change in the peak intensities as shown in **Fig. 3.10.B**. Colorimetric changes corresponding to the ratiometric changes were also examined. Hence, exposing the dispersed AUBM-6-NS in acetonitrile to ultraviolet radiation exhibits no visible emission (I_{317}), in contrast to that of acetone where a pale violet color is observed

(I₄₀₉).

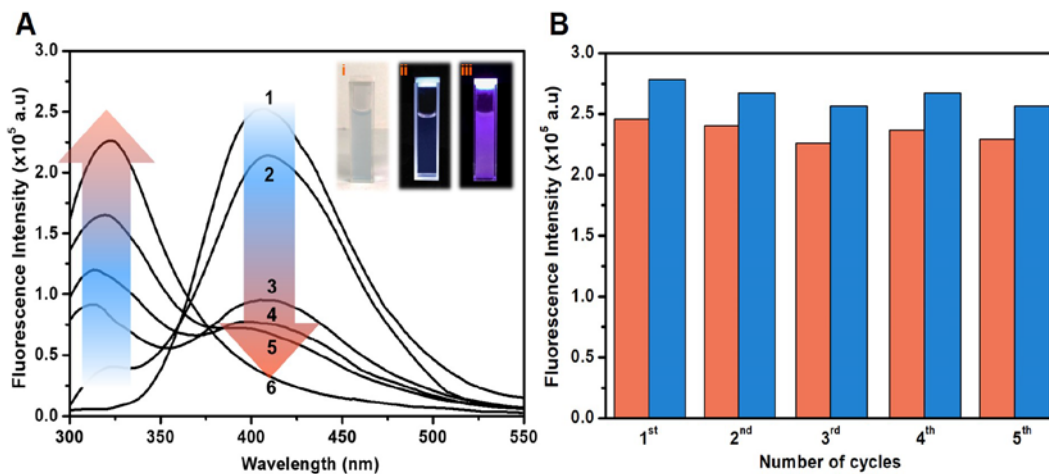


Figure 3.10 (A) Reversibility of ratiometric peaks upon gradual increase in temperature from (1) 25 °C (2) 30 °C (3) 35 °C (4) 40 °C (5) 45 °C (6) 50 °C at $\lambda_{\text{ex}} = 285$ nm. Inset: Colorimetric changes of AUBM-6-NS in (i) acetone under visible light (ii) acetonitrile under ultraviolet light (iii) acetone under ultraviolet light. (B) Recyclability of the ratiometric peaks of AUBM-6-NS after temperature increase (pink: I₃₁₇) and (blue: I₄₀₉)

6. PL-spectra of AUBM-6-NS “turn-off” towards Pd²⁺

Considering the open carboxylate sites present on the INA ligand coordinated within the MOF’s framework, we examined its potential for sensing different metal cations in water. After the dispersion of AUBM-6-NS in acetone, different metal cations having initial concentrations of 2.5 ppm were individually and gradually titrated upon its standard emulsion. As shown in **Fig. 3.11**, most metals examined either had no or a slight significant effect on the PL intensity, except for Pd²⁺, by which a substantial quenching, up to 90% occurred. Initially, the quenching interaction began upon the addition of 0.02 ppm of Pd²⁺, upon which the gradual increase in its concentration resulted in a decrease in its PL intensity reaching a maximum quenching at 0.8 ppm (**Fig. 3.11.C**). Colorimetric changes upon titration of different metal cations at 0.8 ppm was also observed (**Fig. 3.11.D**). Upon the addition of Pd²⁺ ion, the pale violet color disappeared under ultraviolet light illumination as it can be clearly observed by the

naked eye. In contrast, upon the addition of other metal analytes, no considerable change in the color of the solution was noticed.

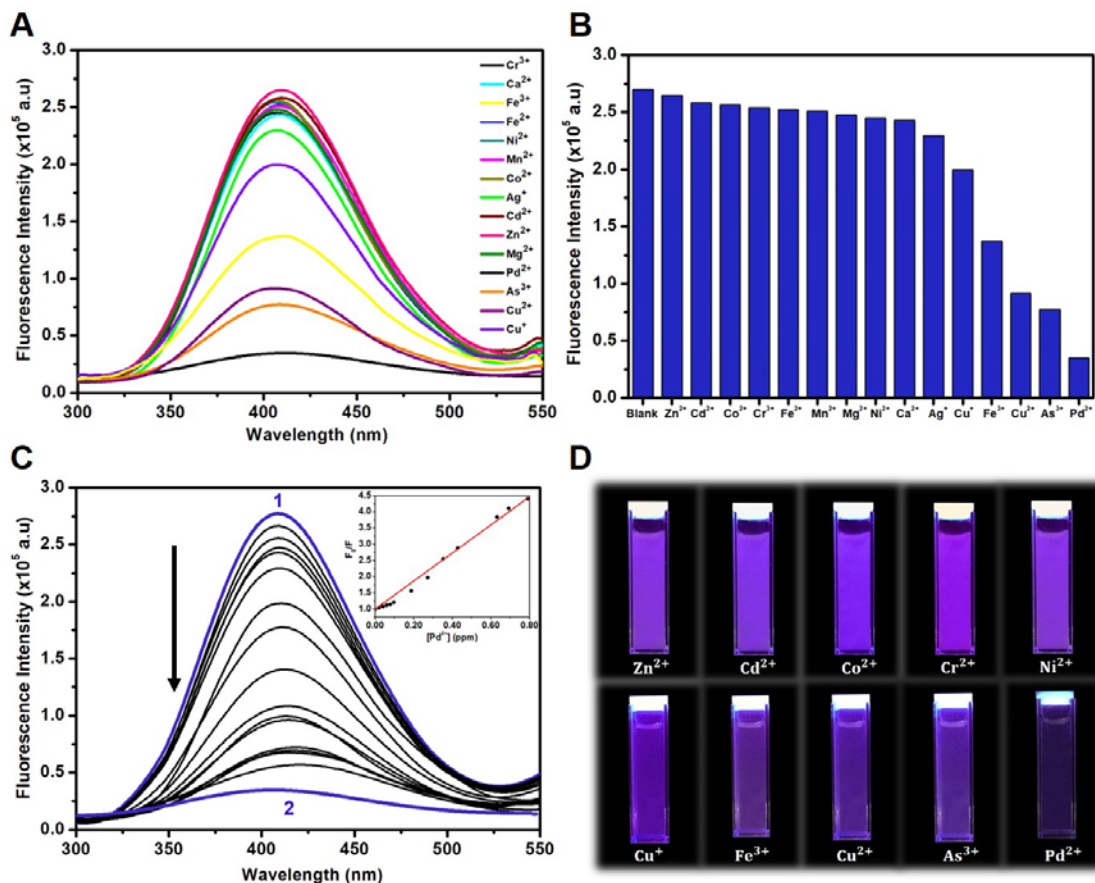


Figure 3.11 (A-B) PL quenching intensities of different metal cations upon addition of 0.8 ppm at $\lambda_{\text{ex}} = 285$ nm. (C) PL spectra of AUBM-6 upon gradual titrations at (1) 0 ppm and (2) 0.8 ppm of Pd²⁺ ions at $\lambda_{\text{ex}} = 285$ nm. Inset: Stern-Volmer plot demonstrating gradual Pd²⁺ titrations (D) Colorimetric changes of AUBM-6-NS is solution upon addition of 0.8 ppm of different metal cations

Analysis of the steady state emission data using the Stern-Volmer plots between F_0/F and $[\text{Pd}^{2+}]$ was employed to determine its K_{sv} value. Consequently, the K_{sv} value obtained upon the gradual addition of Pd²⁺ was determined to be $1.6 \times 10^4 \text{ M}^{-1}$ indicating higher levels of quenching, thus higher levels of sensitivity and binding interactions towards AUBM-6-NS. The obtained K_{sv} values are found to be comparable to other suspension based Pd²⁺ sensors as shown in **Table 3.3**.

Table 3.3 Literature survey about previously reported chemo-sensors towards Pd²⁺ sensing. PA: Picric acid; NA: Not applicable; LOD: Limit of detection

Chemo-sensor	Selectivity	Sensing method	LOD _{min} (ppb)	K _{sv} value (M ⁻¹)	Ref.
Zn-MOF	Fe ³⁺ and Pd ²⁺	turn-off	35	4.2 x 10 ⁴	[¹²¹]
Cd-MOF	Fe ³⁺ and Pd ²⁺	turn-off	18	7.9 x 10 ⁴	[¹²¹]
Zn-MOF	Pd ²⁺ and PA	turn-off	30	3.6 x 10 ⁴	[¹⁰⁷]
Eu-MOF	Pd ²⁺	turn-off	44	7.8 × 10 ⁴	[¹²²]
RPd4	Pd ²⁺	turn-on	50	NA	[¹⁰⁸]
AUBM-6-NS	Pd ²⁺	turn-off	20	1.6 x 10 ⁴	This work

Moreover, the effect of exfoliation on the sensing properties of the MOF was further studied. As shown in **Fig. 3.12**, gradual titrations on emulsions of AUBM-6 showed minimal quenching properties in addition to its relatively lower luminescence intensity compared to that of AUBM-6-NS. This proposes that upon exfoliation, more open binding sites are exposed, which attract more Pd²⁺ ions into the MOF's pores and keep them in close proximity to the conjugated ring present in INA linker, hence causes a perturbation within its electronic structure. Such perturbation causes an alteration in the excited state of the INA linker, which in return inhibits LMCT charge transfer, inducing quenching.

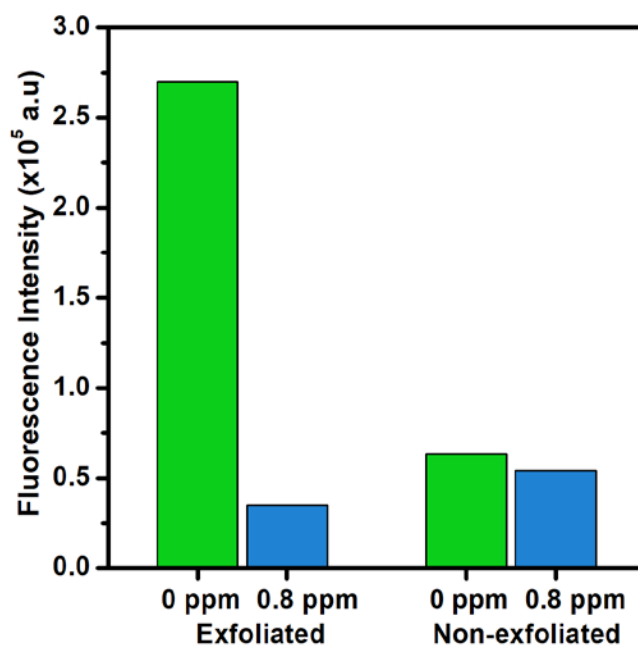


Figure 3.12 Effect of exfoliation on sensing Pd²⁺ at 0.8 ppm of AUBM-6-NS and AUBM-6

In order to understand the selective quenching behaviour of Pd²⁺ towards AUBM-6-NS in the presence of other metal ions, competition experiments were performed as shown in **Fig. 3.13**. Upon the addition of different metal ions at increasing concentrations, none or a slight quenching was observed up to a saturation limit, by which following the addition of Pd²⁺, the PL intensity was completely quenched, hence verifying its remarkable selectivity.

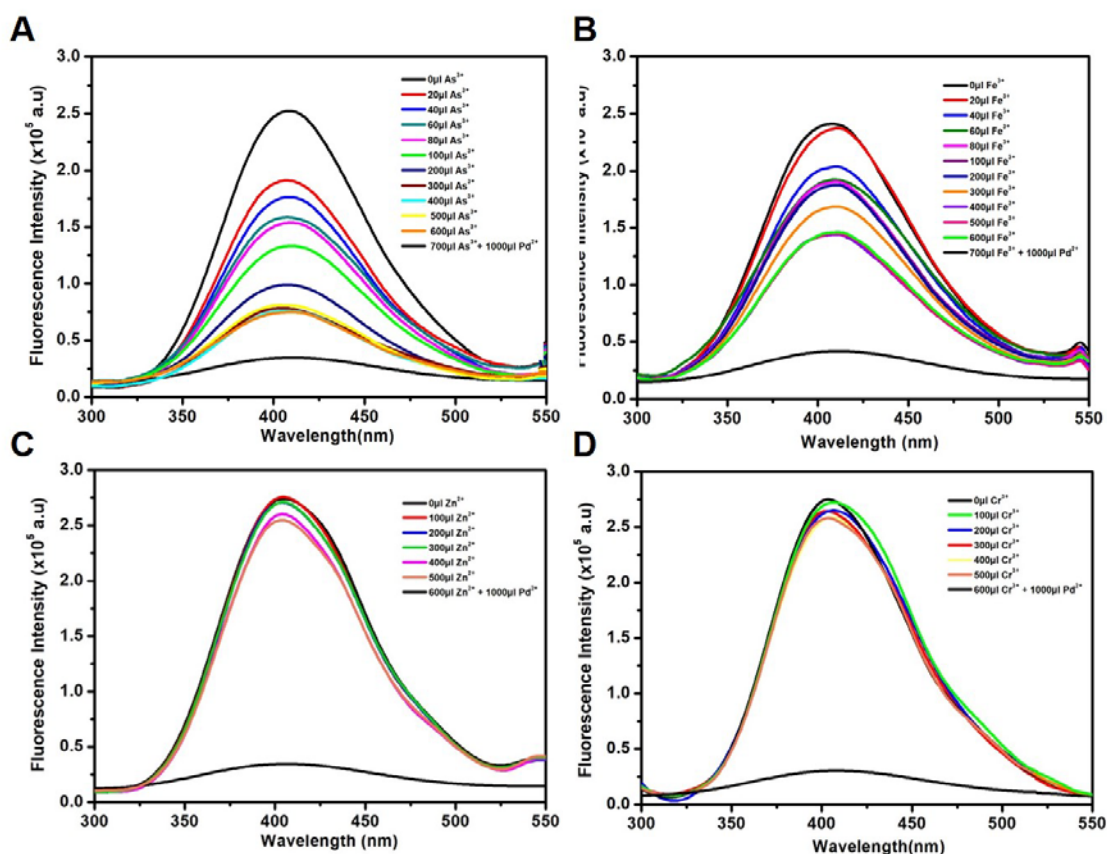


Figure 3.13 The change in fluorescence intensity of AUBM-6-NS in acetone upon addition of (A) As^{3+} (B) Fe^{3+} (C) Zn^{2+} (D) Cr^{3+} followed by 0.8 ppm Pd^{2+} solution.

Furthermore, the effect of pH on the quenching response of AUBM-6-NS towards Pd^{2+} was studied at pH = 4, 6 and 10 (**Fig. 3.14**). Results show that as pH decreases the quenching efficiency was enhanced, where at pH = 4, a 100 % quenching was observed upon addition of 0.57 ppm of Pd^{2+} compared to that of 0.8 ppm at neutral pH. In contrast, as the medium turns basic, quenching efficiency was recorded to decrease. Interestingly, the control experiments demonstrate that the PL of AUBM-6-NS is pH independent, where no change in intensity was observed upon changing the pH value. However, the observed slight decrease in PL intensity of AUBM-6-NS in the latter pH is due to dilution effects (upon addition of 700 μl). In order to explain this enhancement in the quenching behaviour, we investigated the distribution curve of Pd^{2+} species in aqueous solution at different pH.¹²³

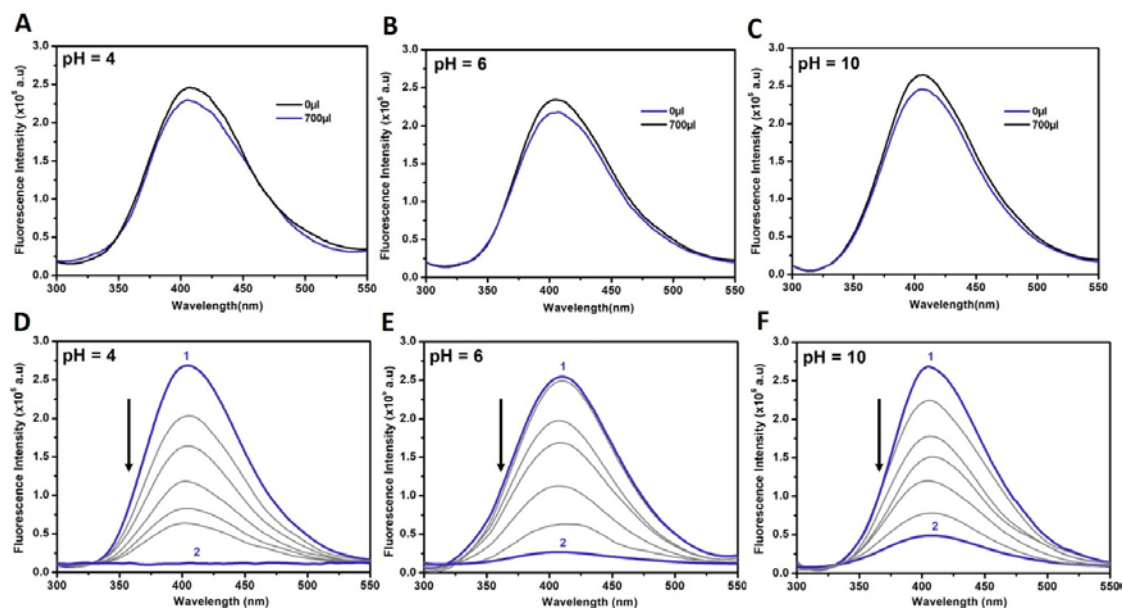
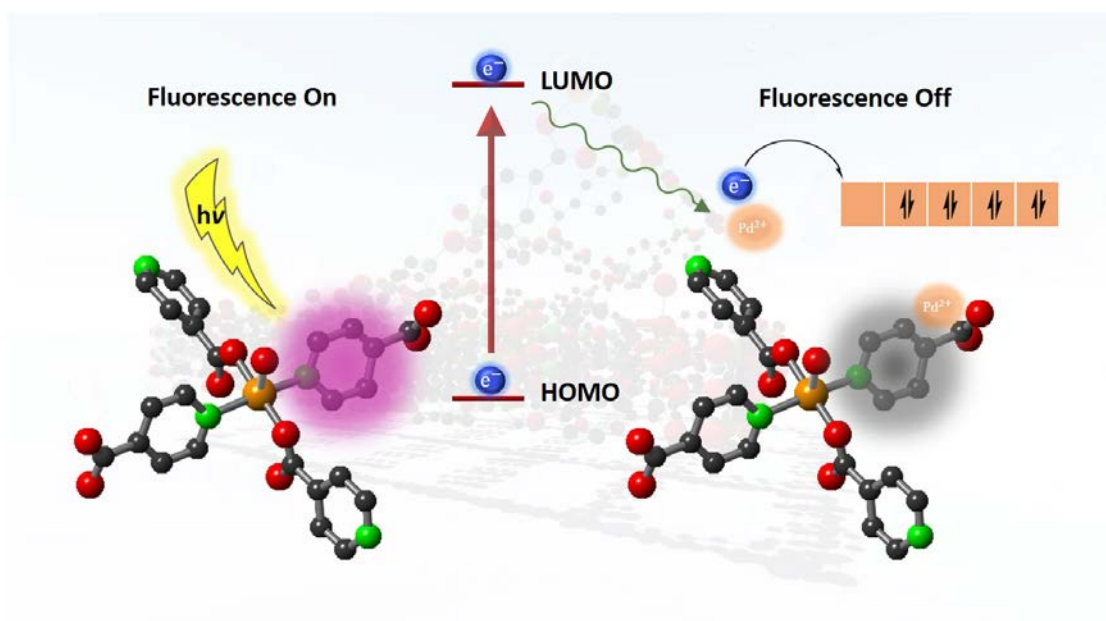


Figure 3.14 (A)(B)(C) Control experiments upon the addition of 700 μl pure solutions without Pd^{2+} ions (D)(E)(F) Quenching experiments having Pd^{2+} ions in corresponding pH solutions upon addition of (1) 0 μl (2) 700 μl .

It can be seen that at high pH (> 8), the hydroxylated species of Pd^{2+} are predominant. Hence, it is concluded that the non-hydroxylated versions have higher affinities towards AUBM-6-NS which resulted in a complete quenching of the PL intensity at pH = 4 at lower concentrations. This shows that Pd^{2+} ion detection is not only sensitive in neutral mediums, but also in acidic environments as well. The sensitivity of AUBM-6-NS towards Pd^{2+} is demonstrated to be among the lowest detected, by which its detection limit was found to be 0.02 ppm which is much beneath the permissible limit set by World Health Organization (WHO) for Pd^{2+} in drug chemicals (5-10 ppm)¹⁰⁵. Moreover, since the Stern-Volmer plot represents a straight line, the presence of dynamic (collisional) quenching is concluded to deactivate the fluorescent excited state of AUBM-6-NS, thus decreasing its luminescent intensity. The proposed mechanism of such quenching relies behind the π -philic nature of Pd^{2+} which may coordinate with the unsaturated alkene moieties ($-\text{CH}=\text{CH}-$) present in INA ligand through (π -d) transitions (Scheme 3.1).



Scheme 3.1 Proposed pathway of the quenching mechanism of AUBM-6-NS upon the addition of Pd²⁺ ions. Copper (gold); Oxygen (red); Nitrogen (green), Carbon (black).

Moreover, according to the Pearson acid-base (HSAB) concept, the pyridine functional group in INA ligand, being a borderline base (electron pair donor) may act to enhance the electron transfer to Pd²⁺ ions that are known to be soft acids (electron pair acceptors)¹²⁴, which in return may explain its high quenching selectivity. The stability of AUBM-6-NS was also studied, by which PXRD pattern of MOF crystals after sensing Pd²⁺ (**Fig. 3.2.A**) was shown to be in agreement with that of the original sample, thus inferring the framework's stability after sensing.

C. Conclusions

A new metal organic framework (AUBM-6) structure is successfully synthesized and fully characterized. The synthesized MOF exhibits a 2D-layered topology that is

activated into its luminescence sensing properties via top down liquid ultrasonication exfoliation of its bulk topology into a few-layer nanosheets. PL investigations of AUBM-6-NS exhibits a ratiometric response towards acetone and a selective and highly sensitive turn-off quenching mechanism towards Pd^{2+} at trace concentrations, even in the presence of competing metal ions. The mutual existence of a ratiometric and turn-off probe suggests the presence of electron transfer mechanisms which demonstrated AUBM-6-NS selectivity towards acetone and Pd^{2+} respectively. The detection of Pd^{2+} was among the lowest reported, which is also below the permissible limits set by WHO. Moreover, the present work may be of great potential demonstrating a dual sensing fluorescent MOF as acetone sensor for medical diagnostics and monitoring, as well as Pd^{2+} ion detection present in reaction vessels thus preventing hazardous environmental and health concerns.

CHAPTER IV

SYNTHESIS AND CHARACTERIZATION OF NEW ONE-DIMENSIONAL METAL–ORGANIC FRAMEWORK AUBM-7

A. Introduction

In this chapter, the successful incorporation of a heterotopic ligand, 2,2':6',2''-terpyridine-4'-carboxylic acid within a new metal organic framework is investigated. Terpyridine ligands have been extensively used in organometallic chemistry, due to their strong impact on coordination chemistry (**Fig. 4.1**).¹²⁵ Having intrinsic lone pairs and low LUMO, nitrogen atoms play a crucial role in providing a strong platform for coordination sites with various metal cations in a nearly planar geometry.¹²⁶⁻¹²⁹ As an NNN-type Pincer ligand, terpyridine provides tight monodentate chelation via each nitrogen with various metal ions including Ru²⁺, Os²⁺, Fe²⁺ or Cd²⁺. Carboxylates, on the other hand, may act as monodentate or bidentate bridging chelating ligands.¹³⁰ The presence of both functionalities within the same ligand enhances the formation of different and unprecedented complexes with various metal ions as is the case with 2,2':6',2''-terpyridine-4'-carboxylic acid (**Fig. 4.1**). Moreover, due to the presence of extended aromatic system within the ligand, intermolecular interactions originating from the delocalization phenomena leads to π – π stacking, which could be relatively strong interactions, consequently exploiting its arrangement from a rather 1D coordination toward 2D or 3D array.¹³¹

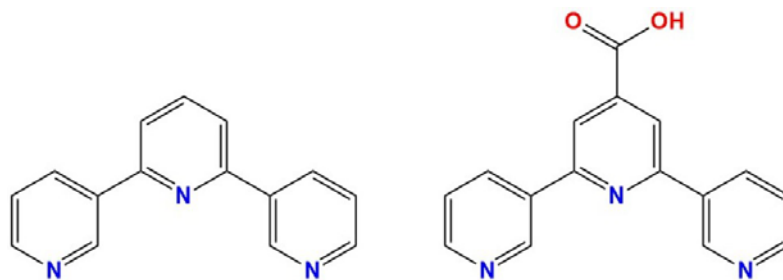


Figure 4.1 2,2':6',2''-terpyridine (left) 2,2':6',2''-terpyridine-4'-carboxylic acid (right).

With the vast library of different complexes reported, it is worthy to note that the incorporation of heterotopic terpyridine linkers within metal–organic frameworks is still a challenge. In 2019, our research group reported the successful incorporation of photoactive bis(4'-(4-carboxyphenyl)-terpyridine)ruthenium(II) linked by Zr atoms that are octahedrally coordinated with O atoms into robust metal–organic framework AUBM-4, as an efficient photocatalyst for carbon dioxide reduction to formate ions under visible light irradiation.⁵⁶ The incorporation of the terpyridine based complexes into the MOF's structure resulted in an enhanced photoactive material in comparison with its Ru(terpyridine) complex and its derivatives.¹³⁰ In addition to its photocatalytic applications, terpyridine-based MOFs have exhibited promising applications in the fields of catalysis, gas adsorption, C-H activation, lanthanide separation and luminescence.¹³²⁻¹³⁷ In this chapter, we report the synthesis and characterization of a novel MOF, incorporating 2,2':6',2''-terpyridine-4'-carboxylic acid as a linker coordinated with Cu(II) ion to form a 1D network extended via π - π stacking to form 3D octahedrally shaped crystals. The resulting green crystals were characterized by single X-ray diffraction analysis, PXRD, TGA, SEM and uv-vis and fluorescence spectroscopy.

B. Results and Discussion

1. Description of Crystal Structure

AUBM-7 crystals exhibit a 1D coordination mode with multi-layered structure topology similar to AUBM-6. As it can be seen in **Fig. 4.2**, single-crystal X-ray diffraction analysis demonstrates that the compound crystallizes in the monoclinic, centrosymmetric space group $P2_1/n$ with lattice parameters of ($a = 8.1981(7) \text{ \AA}$, $b = 14.6320(12) \text{ \AA}$, $c = 11.5208(9) \text{ \AA}$, $\alpha = 90^\circ$, $\beta = 92.297^\circ$, $\gamma = 90^\circ$ and cell volume 1380.86 \AA^3). The symmetric unit cell contains two Cu(II) ions, one crystallographically independent 2,2':6',2''-terpyridine-4'-carboxylic acid (cterpy) and one chloride ion. The acquired molecular formula of the structure is $C_{16}H_{10}CuN_3O_2Cl$. The geometry of the Cu(II) coordination sphere in the MOF structure forms a square pyramidal, where Cu(II) is coordinated to 3 nitrogen atoms of the terpyridine unit and 1 chloride ion forming the square base. The coordination of an oxygen atom from the carboxylate end of a second cterpy ligand orients perpendicularly to the square base forming the square pyramidal geometry. The bond distances of the respective latter coordination ranges for Cu-N 2.051 \AA , Cu-O 2.157 \AA and Cu-Cl 2.254 \AA . The $[Cu\text{-cterpy}]_n$ are bridging through the terpyridine and oxygen atoms in a trans and one-dimensional manner alternatively and extended parallel to the b-axis forming a zigzag-like structure. The subsequent uni-dimensional layers orient in the opposite direction than the previous layer forming the multi-layer structure topology, which are held together by weak intermolecular forces, mainly $\pi\text{-}\pi$ stacking. The layers directed along the a-axis and the distance between consecutive layers ranges between 3.337 \AA and 3.342 \AA taking N-C atoms as reference.

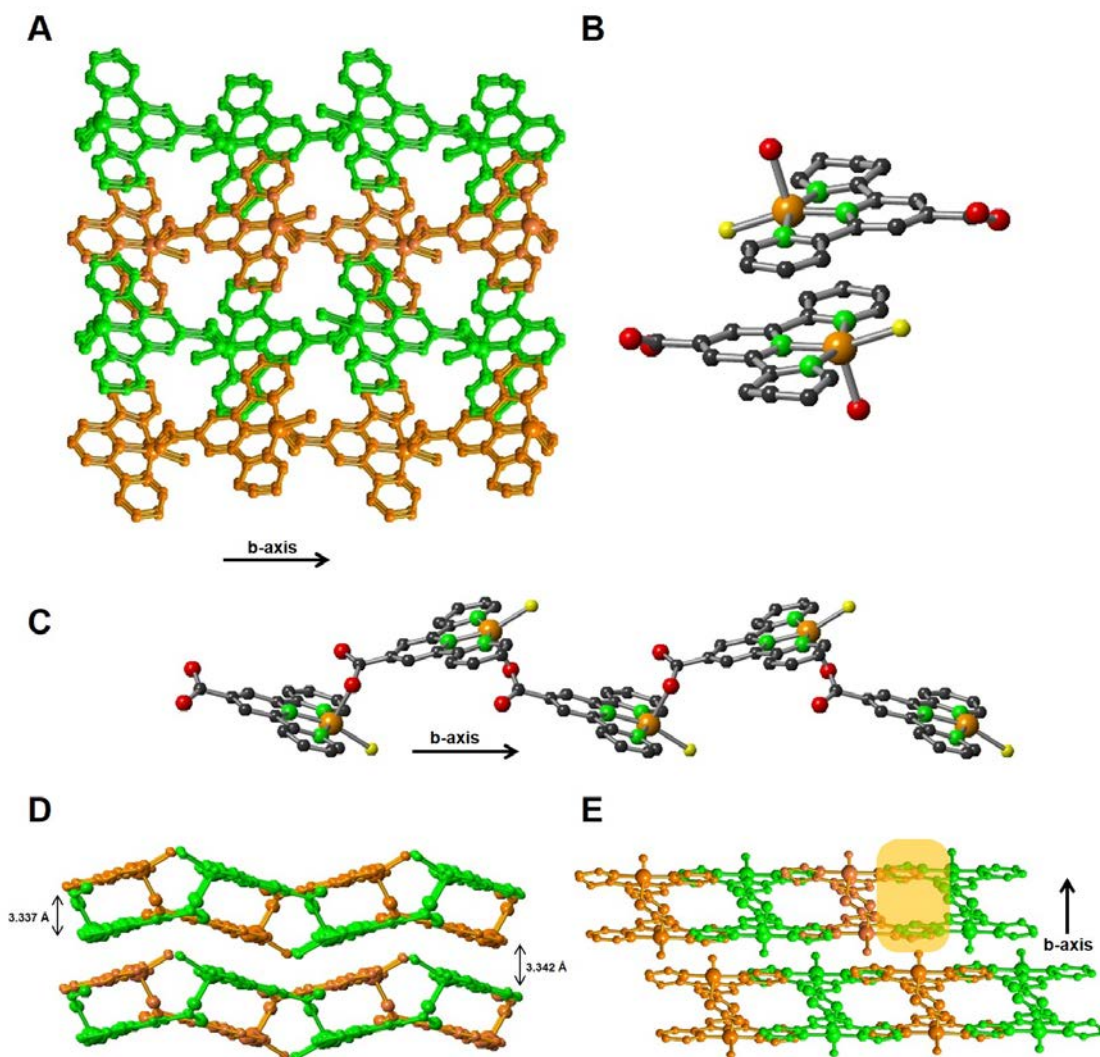


Figure 4.2 (A) Crystal 1-dimensional structure of AUBM-7 (B) Coordination environment and reverse orientation of subsequent multi-layers of AUBM-7. (C) One-dimensional coordination route of AUBM-7 along b-axis (D) Multi-layer view of AUBM-7 (E) π - π stacking of AUBM-7. Copper (gold); Oxygen (red); Nitrogen (green); Carbon (black); Chlorine (yellow).

Table 4.1 Crystal data and structure refinement of AUBM-7

AUBM-7

Empirical formula	$C_{16}H_{10}CuN_3O_2Cl$
Formula weight	375.26
Temperature, K	100
Wavelength, Å	0.71073
Crystal system	Monoclinic

Space group	$P2_1/n$
a, Å	8.1981(7)
b, Å	14.6320(12)
c, Å	11.5208(9)
α , deg	90°
β , deg	92.297(3)°
γ , deg	90°
Volume, Å ³	1380.9(2)
Z	4
Density (calculated), g/cm ³	1.805
Absorption coefficient, mm ⁻¹	1.788
F(000)	756
Index ranges	-14<=h<=14, -26<=k<=26, -20<=l<=20
Reflections collected	8656
Independent reflections	7876 [R(int) = 0.0315]
Completeness to theta = 25.242°	99.0 %
Absorption correction	Multi-scan
Max. and min. transmission	0.748 and 0.700
Refinement method	Full-matrix least-squares on F ²
Goodness-of-fit on F ²	1.109
Extinction coefficient	N/A

2. Powder X-ray Diffraction and Thermogravimetric Analysis

The phase purity of the synthesized AUBM-7 was verified via PXRD by comparing the simulated and experimental patterns. It is noteworthy that the experimental diffraction peaks are shown to be in good agreement with the simulated one (**Fig. 4.3.A**). This verifies the crystalline identity and phase purity of AUBM-7 sample. The thermostability of AUBM-7 was studied by TGA (**Fig. 4.3.B**) within the temperature

range of 30-1000 °C. The TGA curve represents a one-step weight degradation within this temperature range. At 300 °C, there is estimate of 40 % weight loss attributed to the decomposition of organic ligands and the MOF structure.

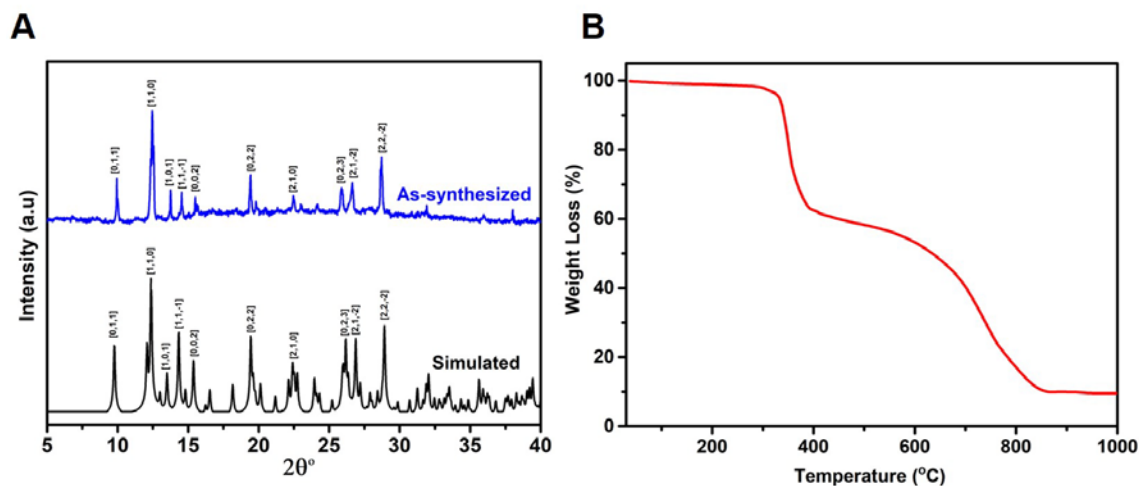


Figure 4.3 (A) PXRD patterns of simulated and as-synthesized samples of AUBM-7. (B) TGA of AUBM-7 between temperature range 30-1000°C.

3. Scanning Electron Microscopy of AUBM-7

AUBM-7 crystals feature polyhedral like shape obtained by stacking of multilayers of [terpy-Cu] as it is demonstrated in **Fig. 4.4**. In contrast to AUBM-6, ultrasonic assisted exfoliation of the bulk layers into few-layer nanosheets could not be carried out under the same experimental conditions. This can be explained by the fact that the displacement of the aromatic rings on top of each other ($\approx 3 \text{ \AA}$) through the strong π - π interactions, stabilize the bulk crystals.¹³⁸ Thus, upon subjecting the crystals to ultrasonication, the breakdown of crystals is observed rather than their exfoliation.

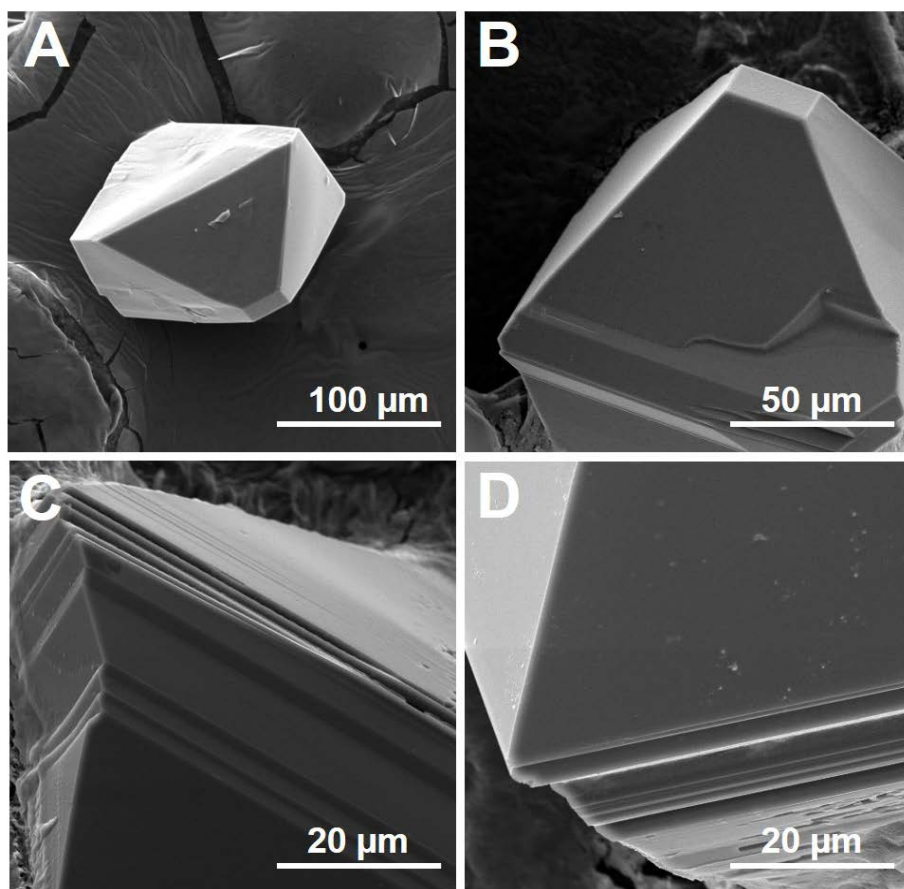


Figure 4.4 SEM images of (A) single crystal of AUBM-7; (B) top view of AUBM-7 single crystal; (C) and (D) multilayers topology of AUBM-7.

4. *Uv-vis and Fluorescence Spectroscopy*

The PL of AUBM-7 was investigated at room temperature. The Uv-vis spectrum of AUBM-6 shows two distinct absorption bands at 250 nm and at 350 nm. At an excitation wavelength of 250 nm, AUBM-7 is shown to have two overlapping shoulder peak emission bands at at 310 nm and 365 nm which are independent from the excitation wavelength, resulting in blue emission. It is concluded that the PL emission spectrum is a partial ligand-based emission due to $\pi-\pi^*$ transitions as it can be seen in **Fig. 4.5**.

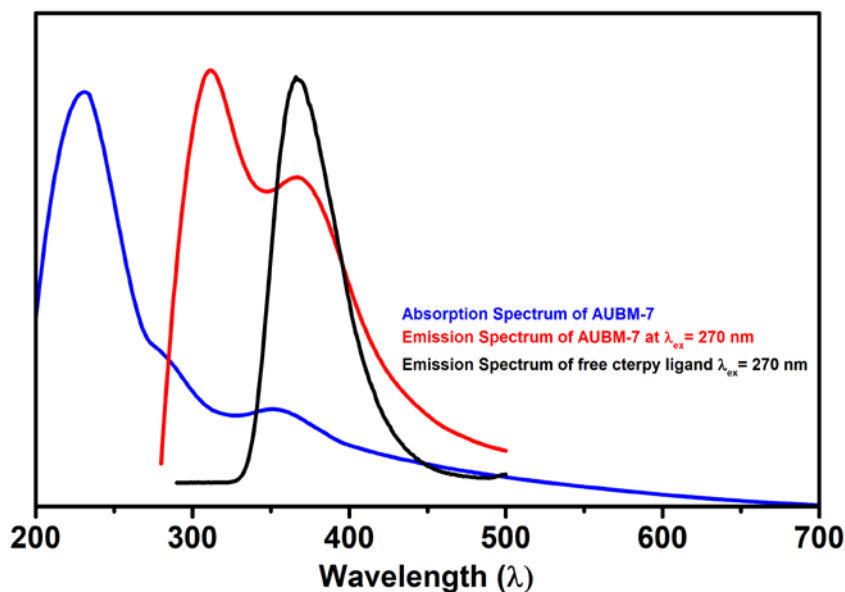


Figure 4.5 Absorption spectrum of AUBM-7 and emission spectra of AUBM-7 and free cterpy ligand at $\lambda_{\text{ex}} = 270$ nm.

C. Conclusions

AUBM-7 was successfully synthesized from 2,2':6',2''-terpyridine-4'-carboxylic acid linker to obtain a 1-dimensional multilayered metal–organic framework. Nevertheless, AUBM-7 have displayed strong intermolecular interactions demonstrated by π – π stacking, yielding a 3-dimensional extended network which prevented their separation into few or multi-layer nanosheets. As shown by single crystal X-ray diffraction, the aromatic rings in the cterpy linker coordinated within the framework are oriented and displaced in a parallel manner with very low separation distance which reinforced such interactions greatly. Potential solvent sensing and metal cation sensing experiments are to be investigated and compared due to the more complex structure of the cterpy linker in comparison to INA ligand.

CHAPTER V

CONCLUDING REMARKS AND FUTURE PERSPECTIVES

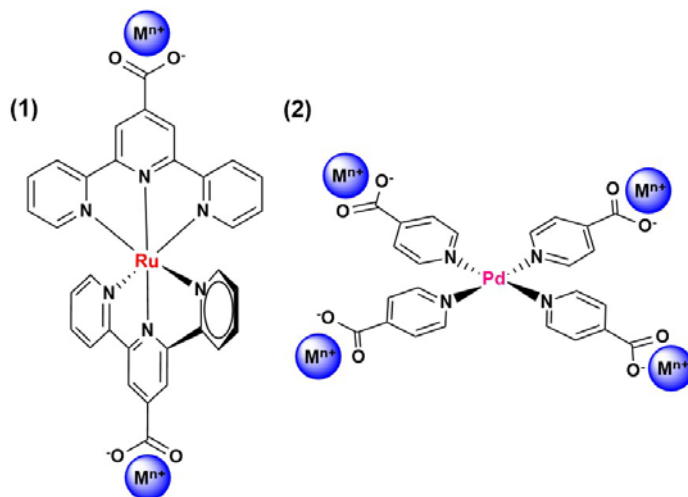
This thesis has covered two projects based on the synthesis and characterization of two novel and Cu(II)-based metal–organic frameworks AUBM-6 and AUBM-7 incorporating heterotopic linkers for chemical sensing applications.

The first portion (Chapter III) demonstrated the successful incorporation of INA linker resulting in a layered 2-dimensional MOF. The four INA linkers were incorporated alternatively via N and O coordinating units, hence utilizing both chelating counterparts of the heterotopic linker within the structural framework. Each layer adopted weakly intermolecular forces held together by hydrogen bonds via the open O site, corresponding to the carboxylate functional group, and water molecules present within the interlayers of the framework. The delamination of the bulk layered AUBM-6 into its ultrathin few layer nanosheets proved to have a successful outcome on enhancing the detection threshold towards ratiometric and turn-off sensing of acetone and Pd(II) respectively. It has also proved to be selective to Pd(II) sensing in the presence of competing metal cations and at acidic pH levels. Up to our knowledge, there has not been a reported transition metal-based MOF exhibiting a ratiometric sensing probe of acetone that is highly sensitive and provides real time monitoring of acetone levels. In the second part (Chapter IV), we explored the incorporation of a more complex heterotopic linker (cterpy) into the framework, resulting in the formation of a 1-dimensional MOF; where Cu(II) ion is linked to cterpy linker on the terpyridine end of one linker and the carboxylate end of the other correspondingly. The coordination is oriented along the b-axis in a zig-zag kind of manner, allowing the π – π stacking of the

phenyl rings between consecutive layers, yielding a 3D extended network. On the contrary to AUBM-6, AUBM-7 did not exhibit similar intermolecular interactions, by which the delamination of the sequential layers could not be performed. The PL properties of AUBM-7 open new doors for the investigation of different chemical sensing applications as an initial attempt to understand further and investigate the proposed mechanisms including the MOF-guest interaction analysis that were present in AUBM-6.

As of future perspectives, since AUBM-6 and AUBM-7 have a square planar base, the incorporation of Pt(II) and Pd(II) is to be inspected by metal exchange reaction or via in-situ synthesis. Such a construct opens new pathways for research applications, by which multivariate systems may act to either enhance or add new functional properties, specifically catalysis. Moreover, the expansion of these frameworks will also be considered, where extended versions of the ligands integrating an additional phenyl ring will be employed to inspect their respective possible pore extension in AUBM-6 and AUBM-7.

Another scenario may arise upon the isolation of different molecular complexes incorporating INA or cterpy and their assimilation within MOFs resulting in a mixed metal system.



For example, isolating cterpy with Ru(III) in a 2:1 ratio (**1**) gives rise to the possibility of integrating another metal on the carboxylate open end of the complex. Similarly, since AUBM-6 exhibits a square planar base geometry, the substitution of Pd(II) or Pt(II) and its isolation into a complex (**2**) may initiate the probability of the incorporation of a different metal forming a mixed metal framework yielding various topological structures.

REFERENCES

1. Yaghi, O. M., Reticular Chemistry—Construction, Properties, and Precision Reactions of Frameworks. *Journal of the American Chemical Society* **2016**, *138* (48), 15507-15509.
2. Yaghi, O. M.; O'Keeffe, M.; Ockwig, N. W.; Chae, H. K.; Eddaoudi, M.; Kim, J., Reticular synthesis and the design of new materials. *Nature* **2003**, *423* (6941), 705-714.
3. Yaghi, O. M.; Kalmutzki, M. J.; Diercks, C. S., *Introduction to Reticular Chemistry Metal-Organic Frameworks and Covalent Organic Frameworks*. Wiley-VCH: 2019.
4. Kraft, A., Wege des Wissens: Berliner Blau, 1706-1726 *Mitteilungen, Gesellschaft Deutscher Chemiker / Fachgruppe Geschichte der Chemie* **2012**.
5. Werner, A., Über 1.2-Dichloro-tetrammin-kobaltisalze (Ammoniak-violeosalze). *European Journal of Inorganic Chemistry* **1907**, *40* (4), 4817-4825.
6. Hoffman, K. A.; Küspert, F., Verbindungen von Kohlenwasserstoffen mit Metallsalzen. *Zeitschrift für anorganische Chemie* **1897**, *15* (1), 204-207.
7. Nishikiori, S.-i.; Iwamoto, T., Crystal structure of Hofmann-dma-type benzene clathrate bis(dimethylamine)cadmium(II) tetracyanonickelate(II) benzene(2/1). *Chemistry Letters* **1984**, *13* (3), 319-322.
8. Robson, R., A net-based approach to coordination polymers *Journal of the Chemical Society, Dalton Transactions* **2000**, (21), 3735-3744.
9. James, S. L., Metal-organic frameworks. *Chemical Society Reviews* **2003**, *32* (5), 276-288.
10. Li, H.; Eddaoudi, M.; Groy, T. L.; Yaghi, O. M., Establishing Microporosity in Open Metal-Organic Frameworks: Gas Sorption Isotherms for Zn(BDC) (BDC) 1,4-Benzenedicarboxylate). *Journal of the American Chemical Society* **1998**, *120* (33), 8571-8572.
11. Yaghi, O. M.; Li, H., Hydrothermal Synthesis of a Metal-Organic Framework Containing Large Rectangular Channels. *Journal of the American Chemical Society* **1995**, *117* (41), 10401-10402.
12. Moghadam, P. Z.; Li, A.; Wiggin, S. B.; Tao, A.; Maloney, A. G. P.; Wood, P. A.; Ward, S. C.; Fairen-Jimenez, D., Development of a Cambridge Structural Database Subset: A Collection of Metal–Organic Frameworks for Past, Present, and Future. *Chemistry of Materials* **2017**, *29* (7), 2618-2625.
13. Rosswell, J. L. C.; Yaghi, O. M., Metal–organic frameworks: a new class of porous materials. *Microporous and Mesoporous Materials* **2004**, *73*, 3-14.
14. Wells, A., The geometrical basis of crystal chemistry. Part 1. *Acta Crystallographica* **1954**, *7* (8-9), 535-544.
15. Eddaoudi, M.; Moler, D. B.; Li, H.; Chen, B.; Reineke, T. M.; O'Keeffe, M.; Yaghi, O. M., Modular Chemistry: Secondary Building Units as a Basis for the Design of Highly Porous and Robust Metal–Organic Carboxylate Frameworks. *Accounts of Chemical Research* **2001**, *34* (4), 319-330.
16. Kalmutzki, M. J.; Hanikel, N.; Yaghi, O. M., Secondary building units as the turning point in the development of the reticular chemistry of MOFs. *Science Advances* **2018**, *4* (10), eaat9180.

17. Baerlocher, C.; Meier, W. M.; Olson, D. H., Atlas of Zeolite Framework Types. In *Atlas of Zeolite Framework Types*, Baerlocher, C.; Meier, W. M.; Olson, D. H., Eds. Elsevier: Amsterdam, 2001; pp 1-2.
18. Clegg, W.; Cressey, J. T.; Harbron, D. R.; Straughan, B. P., Polymeric and mixed carboxylate compounds: Crystal structures of $[\text{Zn}(\text{tiglate})_2]_x$ and $[\text{Zn}_2(\text{tiglate})_3(\text{crotonate})]_x$. *Journal of Chemical Crystallography* **1994**, *24* (3), 211-217.
19. Clegg, W.; Little, I. R.; Straughan, B. P., Zinc carboxylate complexes: structural characterisation of some binuclear and linear trinuclear complexes. *Journal of the Chemical Society, Dalton Transactions* **1986**, (6), 1283-1288.
20. Jiafei, L.; Xuan, Z.; Zhijie, C.; Ryther, A.; Xingjie, W.; Megan C., W.; Peng, B.; Xianghai, G.; Timur, I.; Diego, G.-G.; Omar K., F., *Orthogonal Synthesis of Highly Porous Zr-MOFs Assembled from Simple Building Blocks for Oxygen Storage*. 2019.
21. Islamoglu, T.; Otake, K.-i.; Li, P.; Buru, C. T.; Peters, A. W.; Akpinar, I.; Garibay, S. J.; Farha, O. K., Revisiting the structural homogeneity of NU-1000, a Zr-based metal-organic framework. *CrystEngComm* **2018**, *20* (39), 5913-5918.
22. Richens, D. T., Ligand Substitution Reactions at Inorganic Centers. *Chem Rev* **2005**, *105* (6), 1961-2002.
23. Tranchemontagne, D. J.; Mendoza-Cortés, J. L.; O’Keeffe, M.; Yaghi, O. M., Secondary building units, nets and bonding in the chemistry of metal-organic frameworks. *Chemical Society Reviews* **2009**, *38* (5), 1257-1283.
24. Yuan, S.; Feng, L.; Wang, K.; Pang, J.; Bosch, M.; Lollar, C.; Sun, Y.; Qin, J.; Yang, X.; Zhang, P.; Wang, Q.; Zou, L.; Zhang, Y.; Zhang, L.; Fang, Y.; Li, J.; Zhou, H.-C., Stable Metal-Organic Frameworks: Design, Synthesis, and Applications. *Advanced Materials* **2018**, *30* (37), 1704303.
25. Cook, T. R.; Zheng, Y.-R.; Stang, P. J., Metal-organic frameworks and self-assembled supramolecular coordination complexes: comparing and contrasting the design, synthesis, and functionality of metal-organic materials. *Chem Rev* **2013**, *113* (1), 734-777.
26. Guo, X.-Z.; Chen, S.-S.; Li, W.-D.; Han, S.-S.; Deng, F.; Qiao, R.; Zhao, Y., Series of Cadmium(II) Coordination Polymers Based on a Versatile Multi-N-Donor Tecton or Mixed Carboxylate Ligands: Synthesis, Structure, and Selectively Sensing Property. *ACS Omega* **2019**, *4* (7), 11540-11553.
27. Schoedel, A.; Yaghi, O., Porosity in Metal-Organic Compounds: How Izatt-Christensen Award Winners Shaped the Field. 2016; pp 200-219.
28. Li, H.; Eddaoudi, M.; Groy, T. L.; Yaghi, O. M., Establishing Microporosity in Open Metal-Organic Frameworks: Gas Sorption Isotherms for Zn(BDC) (BDC = 1,4-Benzenedicarboxylate). *Journal of the American Chemical Society* **1998**, *120* (33), 8571-8572.
29. Clegg, W.; Harbron, D. R.; Homan, C. D.; Hunt, P. A.; Little, I. R.; Straughan, B. P., Crystal structures of three basic zinc carboxylates together with infrared and FAB mass spectrometry studies in solution. *Inorganica Chimica Acta* **1991**, *186* (1), 51-60.
30. Eddaoudi, M.; Kim, J.; Rosi, N.; Vodak, D.; Wachter, J.; O’Keeffe, M.; Yaghi, O. M., Systematic Design of Pore Size and Functionality in Isoreticular MOFs and Their Application in Methane Storage. *Science (New York, N.Y.)* **2002**, *295* (5554), 469-472.
31. Ma, L.; Jin, A.; Xie, Z.; Lin, W., Freeze drying significantly increases permanent porosity and hydrogen uptake in 4,4-connected metal-organic frameworks. *Angewandte Chemie (International ed. in English)* **2009**, *48* (52), 9905-8.

32. Nelson, A. P.; Farha, O. K.; Mulfort, K. L.; Hupp, J. T., Supercritical Processing as a Route to High Internal Surface Areas and Permanent Microporosity in Metal–Organic Framework Materials. *Journal of the American Chemical Society* **2009**, *131* (2), 458-460.
33. Park, Y. K.; Choi, S. B.; Kim, H.; Kim, K.; Won, B. H.; Choi, K.; Choi, J. S.; Ahn, W. S.; Won, N.; Kim, S.; Jung, D. H.; Choi, S. H.; Kim, G. H.; Cha, S. S.; Jhon, Y. H.; Yang, J. K.; Kim, J., Crystal structure and guest uptake of a mesoporous metal-organic framework containing cages of 3.9 and 4.7 nm in diameter. *Angewandte Chemie (International ed. in English)* **2007**, *46* (43), 8230-3.
34. Duan, P.; Moreton, J. C.; Tavares, S. R.; Semino, R.; Maurin, G.; Cohen, S. M.; Schmidt-Rohr, K., Polymer Infiltration into Metal–Organic Frameworks in Mixed-Matrix Membranes Detected in Situ by NMR. *Journal of the American Chemical Society* **2019**, *141* (18), 7589-7595.
35. Kitao, T.; Zhang, Y.; Kitagawa, S.; Wang, B.; Uemura, T., Hybridization of MOFs and polymers. *Chemical Society Reviews* **2017**, *46* (11), 3108-3133.
36. Uemura, T.; Yanai, N.; Kitagawa, S., Polymerization reactions in porous coordination polymers. *Chemical Society Reviews* **2009**, *38* (5), 1228-1236.
37. Uemura, T.; Yanai, N.; Watanabe, S.; Tanaka, H.; Numaguchi, R.; Miyahara, M. T.; Ohta, Y.; Nagaoka, M.; Kitagawa, S., Unveiling thermal transitions of polymers in subnanometre pores. *Nature communications* **2010**, *1*, 83.
38. Peng, L.; Yang, S.; Jawahery, S.; Moosavi, S. M.; Huckaba, A. J.; Asgari, M.; Oveisi, E.; Nazeeruddin, M. K.; Smit, B.; Queen, W. L., Preserving Porosity of Mesoporous Metal–Organic Frameworks through the Introduction of Polymer Guests. *Journal of the American Chemical Society* **2019**, *141* (31), 12397-12405.
39. Almeida Paz, F. A.; Klinowski, J.; Vilela, S. M. F.; Tomé, J. P. C.; Cavaleiro, J. A. S.; Rocha, J., Ligand design for functional metal–organic frameworks. *Chemical Society Reviews* **2012**, *41* (3), 1088-1110.
40. Lu, W.; Wei, Z.; Gu, Z.-Y.; Liu, T.-F.; Park, J.; Park, J.; Tian, J.; Zhang, M.; Zhang, Q.; Gentle Iii, T.; Bosch, M.; Zhou, H.-C., Tuning the structure and function of metal–organic frameworks via linker design. *Chemical Society Reviews* **2014**, *43* (16), 5561-5593.
41. Catarineu, N. R.; Schoedel, A.; Urban, P.; Morla, M. B.; Trickett, C. A.; Yaghi, O. M., Two Principles of Reticular Chemistry Uncovered in a Metal–Organic Framework of Heterotritopic Linkers and Infinite Secondary Building Units. *Journal of the American Chemical Society* **2016**, *138* (34), 10826-10829.
42. Lee, S. J.; Doussot, C.; Baux, A.; Liu, L.; Jameson, G. B.; Richardson, C.; Pak, J. J.; Trouselet, F.; Coudert, F.-X.; Telfer, S. G., Multicomponent Metal–Organic Frameworks as Defect-Tolerant Materials. *Chemistry of Materials* **2016**, *28* (1), 368-375.
43. Furukawa, H.; Müller, U.; Yaghi, O. M., “Heterogeneity within Order” in Metal–Organic Frameworks. *Angewandte Chemie International Edition* **2015**, *54* (11), 3417-3430.
44. Dong, X.-Y.; Wang, R.; Li, J.-B.; Zang, S.-Q.; Hou, H.-W.; Mak, T. C. W., A tetranuclear Cu₄(μ₃-OH)₂-based metal–organic framework (MOF) with sulfonate–carboxylate ligands for proton conduction. *Chemical Communications* **2013**, *49* (90), 10590-10592.
45. Lincke, J.; Lässig, D.; Kobalz, M.; Bergmann, J.; Handke, M.; Möllmer, J.; Lange, M.; Roth, C.; Möller, A.; Staudt, R.; Krautscheid, H., An Isomorphous Series of

- Cubic, Copper-Based Triazolyl Isophthalate MOFs: Linker Substitution and Adsorption Properties. *Inorganic Chemistry* **2012**, *51* (14), 7579-7586.
46. Quartapelle Procopio, E.; Linares, F.; Montoro, C.; Colombo, V.; Maspero, A.; Barea, E.; Navarro, J. A. R., Cation-Exchange Porosity Tuning in Anionic Metal–Organic Frameworks for the Selective Separation of Gases and Vapors and for Catalysis. *Angewandte Chemie International Edition* **2010**, *49* (40), 7308-7311.
47. Li, M.; Li, D.; O’Keeffe, M.; Yaghi, O. M., Topological Analysis of Metal–Organic Frameworks with Polytopic Linkers and/or Multiple Building Units and the Minimal Transitivity Principle. *Chem Rev* **2014**, *114* (2), 1343-1370.
48. Tu, B.; Pang, Q.; Xu, H.; Li, X.; Wang, Y.; Ma, Z.; Weng, L.; Li, Q., Reversible Redox Activity in Multicomponent Metal–Organic Frameworks Constructed from Trinuclear Copper Pyrazolate Building Blocks. *Journal of the American Chemical Society* **2017**, *139* (23), 7998-8007.
49. Tu, B.; Pang, Q.; Ning, E.; Yan, W.; Qi, Y.; Wu, D.; Li, Q., Heterogeneity within a Mesoporous Metal–Organic Framework with Three Distinct Metal-Containing Building Units. *Journal of the American Chemical Society* **2015**, *137* (42), 13456-13459.
50. Deng, H.; Doonan, C. J.; Furukawa, H.; Ferreira, R. B.; Towne, J.; Knobler, C. B.; Wang, B.; Yaghi, O. M., Multiple functional groups of varying ratios in metal-organic frameworks. *Science (New York, N.Y.)* **2010**, *327* (5967), 846-50.
51. Botas, J. A.; Calleja, G.; Sanchez-Sanchez, M.; Orcajo, M. G., Cobalt doping of the MOF-5 framework and its effect on gas-adsorption properties. *Langmuir : the ACS journal of surfaces and colloids* **2010**, *26* (8), 5300-3.
52. Rosi, N. L.; Kim, J.; Eddaoudi, M.; Chen, B.; O’Keeffe, M.; Yaghi, O. M., Rod Packings and Metal–Organic Frameworks Constructed from Rod-Shaped Secondary Building Units. *Journal of the American Chemical Society* **2005**, *127* (5), 1504-1518.
53. Wang, L. J.; Deng, H.; Furukawa, H.; Gándara, F.; Cordova, K. E.; Peri, D.; Yaghi, O. M., Synthesis and Characterization of Metal–Organic Framework-74 Containing 2, 4, 6, 8, and 10 Different Metals. *Inorganic Chemistry* **2014**, *53* (12), 5881-5883.
54. Asgari, M.; Jawahery, S.; Bloch, E. D.; Hudson, M. R.; Flacau, R.; Vlaisavljevich, B.; Long, J. R.; Brown, C. M.; Queen, W. L., An experimental and computational study of CO₂ adsorption in the sodalite-type M-BTT (M = Cr, Mn, Fe, Cu) metal–organic frameworks featuring open metal sites. *Chemical Science* **2018**, *9* (20), 4579-4588.
55. DeCoste, J. B.; Denny, J. M. S.; Peterson, G. W.; Mahle, J. J.; Cohen, S. M., Enhanced aging properties of HKUST-1 in hydrophobic mixed-matrix membranes for ammonia adsorption. *Chemical Science* **2016**, *7* (4), 2711-2716.
56. Elcheikh Mahmoud, M.; Audi, H.; Assoud, A.; Ghaddar, T. H.; Hmadeh, M., Metal–Organic Framework Photocatalyst Incorporating Bis(4’-(4-carboxyphenyl)-terpyridine)ruthenium(II) for Visible-Light-Driven Carbon Dioxide Reduction. *Journal of the American Chemical Society* **2019**, *141* (17), 7115-7121.
57. Horcajada, P.; Serre, C.; Vallet-Regi, M.; Sebban, M.; Taulelle, F.; Ferey, G., Metal-organic frameworks as efficient materials for drug delivery. *Angewandte Chemie (International ed. in English)* **2006**, *45* (36), 5974-8.
58. Sun, D. T.; Gasilova, N.; Yang, S.; Oveisi, E.; Queen, W. L., Rapid, Selective Extraction of Trace Amounts of Gold from Complex Water Mixtures with a Metal–Organic Framework (MOF)/Polymer Composite. *Journal of the American Chemical Society* **2018**, *140* (48), 16697-16703.

59. Xu, H.; Liu, F.; Cui, Y.; Chen, B.; Qian, G., A luminescent nanoscale metal–organic framework for sensing of nitroaromatic explosives. *Chemical Communications* **2011**, 47 (11), 3153-3155.
60. Li, J. R.; Kuppler, R. J.; Zhou, H. C., Selective gas adsorption and separation in metal-organic frameworks. *Chem Soc Rev* **2009**, 38 (5), 1477-504.
61. Kreno, L. E.; Leong, K.; Farha, O. K.; Allendorf, M.; Van Duyne, R. P.; Hupp, J. T., Metal–Organic Framework Materials as Chemical Sensors. *Chem Rev* **2012**, 112 (2), 1105-1125.
62. Allendorf, M. D.; Bauer, C. A.; Bhakta, R. K.; Houk, R. J. T., Luminescent metal–organic frameworks. *Chemical Society Reviews* **2009**, 38 (5), 1330-1352.
63. Wang, S.; Ding, H.; Wang, Y.; Fan, C.; Liu, G.; Pu, S., A colorimetric and ratiometric fluorescent sensor for sequentially detecting Cu²⁺ and arginine based on a coumarin–rhodamine B derivative and its application for bioimaging. *RSC Advances* **2019**, 9 (12), 6643-6649.
64. Lustig, W. P.; Mukherjee, S.; Rudd, N. D.; Desai, A. V.; Li, J.; Ghosh, S. K., Metal–organic frameworks: functional luminescent and photonic materials for sensing applications. *Chemical Society Reviews* **2017**, 46 (11), 3242-3285.
65. Yu, Y.; Ma, J.-P.; Dong, Y.-B., Luminescent humidity sensors based on porous Ln³⁺-MOFs. *CrystEngComm* **2012**, 14 (21), 7157-7160.
66. Ma, D.; Li, B.; Zhou, X.; Zhou, Q.; Liu, K.; Zeng, G.; Li, G.; Shi, Z.; Feng, S., A dual functional MOF as a luminescent sensor for quantitatively detecting the concentration of nitrobenzene and temperature. *Chemical Communications* **2013**, 49 (79), 8964-8966.
67. Lin, R. B.; Liu, S. Y.; Ye, J. W.; Li, X. Y.; Zhang, J. P., Photoluminescent metal–organic frameworks for gas sensing. *Advanced Science* **2016**, 3 (7), 1500434.
68. Wu, Z.-F.; Tan, B.; Velasco, E.; Wang, H.; Shen, N.-N.; Gao, Y.-J.; Zhang, X.; Zhu, K.; Zhang, G.-Y.; Liu, Y.-Y.; Hei, X.-Z.; Huang, X.-Y.; Li, J., Fluorescent In based MOFs showing “turn on” luminescence towards thiols and acting as a ratiometric fluorescence thermometer. *Journal of Materials Chemistry C* **2019**, 7 (10), 3049-3055.
69. Dincă, M.; Long, J. R., Strong H₂ Binding and Selective Gas Adsorption within the Microporous Coordination Solid Mg₃(O₂C-C₁₀H₆-CO₂)₃. *Journal of the American Chemical Society* **2005**, 127 (26), 9376-9377.
70. Xiang, Z.; Fang, C.; Leng, S.; Cao, D., An amino group functionalized metal–organic framework as a luminescent probe for highly selective sensing of Fe³⁺ ions. *Journal of Materials Chemistry A* **2014**, 2 (21), 7662-7665.
71. Xu, H.; Dong, Y.; Wu, Y.; Ren, W.; Zhao, T.; Wang, S.; Gao, J., An -OH group functionalized MOF for ratiometric Fe³⁺ sensing. *Journal of Solid State Chemistry* **2018**, 258, 441-446.
72. Fan, J.; Zhu, H.-F.; Okamura, T.-a.; Sun, W.-Y.; Tang, W.-X.; Ueyama, N., Three-dimensional photoluminescent pillared metal-organic framework with 4.82 topological channels obtained from the assembly of cadmium(ii) acetate and trimellitic salt. *New Journal of Chemistry* **2003**, 27 (10), 1409-1411.
73. Pan, L.; Zheng, N.; Wu, Y.; Han, S.; Yang, R.; Huang, X.; Li, J., Synthesis, Characterization and Structural Transformation of A Condensed Rare Earth Metal Coordination Polymer. *Inorganic Chemistry* **2001**, 40 (5), 828-830.
74. Hassan, G. F.; El Hoda Saad, N.; Hmadeh, M.; Karam, P., Enhancing porphyrin photostability when locked in metal–organic frameworks. *Dalton Transactions* **2018**, 47 (44), 15765-15771.

75. Sobbi, A. K.; Wöhrle, D.; Schlettwein, D., Photochemical stability of various porphyrins in solution and as thin film electrodes. *Journal of the Chemical Society, Perkin Transactions 2* **1993**, (3), 481-488.
76. Zhao, S.-S.; Zhang, H.; Wang, L.; Chen, L.; Xie, Z., Facile preparation of a tetraphenylethylene-doped metal-organic framework for white light-emitting diodes. *Journal of Materials Chemistry C* **2018**, 6 (43), 11701-11706.
77. Li, Y. L.; Zhao, Y.; Wang, P.; Kang, Y. S.; Liu, Q.; Zhang, X. D.; Sun, W. Y., Multifunctional Metal-Organic Frameworks with Fluorescent Sensing and Selective Adsorption Properties. *Inorg Chem* **2016**, 55 (22), 11821-11830.
78. Cui, P. P.; Zhang, X. D.; Wang, P.; Zhao, Y.; Azam, M.; Al-Resayes, S. I.; Sun, W. Y., Zinc(II) and Copper(II) Hybrid Frameworks via Metal-Ion Metathesis with Enhanced Gas Uptake and Photoluminescence Properties. *Inorg Chem* **2017**, 56 (22), 14157-14163.
79. Dong, J.; Zhao, D.; Lu, Y.; Sun, W.-Y., Photoluminescent metal-organic frameworks and their application for sensing biomolecules. *Journal of Materials Chemistry A* **2019**, 7 (40), 22744-22767.
80. Takashima, Y.; Martínez, V. M.; Furukawa, S.; Kondo, M.; Shimomura, S.; Uehara, H.; Nakahama, M.; Sugimoto, K.; Kitagawa, S., Molecular decoding using luminescence from an entangled porous framework. *Nature communications* **2011**, 2, 168.
81. Jensen, S.; Tan, K.; Lustig, W. P.; Kilin, D. S.; Li, J.; Chabal, Y. J.; Thonhauser, T., Structure-Driven Photoluminescence Enhancement in a Zn-Based Metal-Organic Framework. *Chemistry of Materials* **2019**, 31 (19), 7933-7940.
82. Liu, X.-Y.; Li, Y.; Tsung, C.-K.; Li, J., Encapsulation of yellow phosphors into nanocrystalline metal-organic frameworks for blue-excitable white light emission. *Chemical Communications* **2019**, 55 (72), 10669-10672.
83. Nigam, S.; Rutan, S., Principles and Applications of Solvatochromism. *Appl. Spectrosc.* **2001**, 55 (11), 362A-370A.
84. Reineke, T. M.; Eddaoudi, M.; Fehr, M.; Kelley, D.; Yaghi, O. M., From Condensed Lanthanide Coordination Solids to Microporous Frameworks Having Accessible Metal Sites. *Journal of the American Chemical Society* **1999**, 121 (8), 1651-1657.
85. Basabe-Desmonts, L.; Reinhoudt, D. N.; Crego-Calama, M., Design of fluorescent materials for chemical sensing. *Chemical Society Reviews* **2007**, 36 (6), 993-1017.
86. Rieter, W. J.; Taylor, K. M. L.; An, H.; Lin, W.; Lin, W., Nanoscale Metal-Organic Frameworks as Potential Multimodal Contrast Enhancing Agents. *Journal of the American Chemical Society* **2006**, 128 (28), 9024-9025.
87. Chen, L.; Liu, D.; Peng, J.; Du, Q.; He, H., Ratiometric fluorescence sensing of metal-organic frameworks: Tactics and perspectives. *Coordination Chemistry Reviews* **2020**, 404, 213113.
88. Bigdeli, A.; Ghasemi, F.; Abbasi-Moayed, S.; Shahrajabian, M.; Fahimi-Kashani, N.; Jafarinejad, S.; Farahmand Nejad, M. A.; Hormozi-Nezhad, M. R., Ratiometric fluorescent nanoprobe for visual detection: Design principles and recent advances - A review. *Analytica Chimica Acta* **2019**, 1079, 30-58.
89. Luo, H.-Y.; Jiang, J.-H.; Zhang, X.-B.; Li, C.-Y.; Shen, G.-L.; Yu, R.-Q., Synthesis of porphyrin-appended terpyridine as a chemosensor for cadmium based on fluorescent enhancement. *Talanta* **2007**, 72 (2), 575-581.

90. Moghadam, P. Z.; Islamoglu, T.; Goswami, S.; Exley, J.; Fantham, M.; Kaminski, C. F.; Snurr, R. Q.; Farha, O. K.; Fairen-Jimenez, D., Computer-aided discovery of a metal-organic framework with superior oxygen uptake. *Nature communications* **2018**, *9* (1), 1378.
91. Jrad, A.; Abu Tarboush, B. J.; Hmadeh, M.; Ahmad, M., Tuning acidity in zirconium-based metal organic frameworks catalysts for enhanced production of butyl butyrate. *Applied Catalysis A: General* **2019**, *570*, 31-41.
92. Atallah, H.; M, E. L. M.; Jelle, A.; Lough, A.; Hmadeh, M., A highly stable indium based metal organic framework for efficient arsenic removal from water. *Dalton transactions (Cambridge, England : 2003)* **2018**, *47* (3), 799-806.
93. Rowsell, J. L. C.; Yaghi, O. M., Metal-organic frameworks: a new class of porous materials. *Microporous and Mesoporous Materials* **2004**, *73* (1), 3-14.
94. Zhou, H.-C. J.; Kitagawa, S., Metal-Organic Frameworks (MOFs). *Chemical Society Reviews* **2014**, *43* (16), 5415-5418.
95. Rosi, N. L.; Eddaoudi, M.; Kim, J.; O'Keeffe, M.; Yaghi, O. M., Advances in the chemistry of metal-organic frameworks. *CrystEngComm* **2002**, *4* (68), 401-404.
96. Cui, Y.; Xu, H.; Yue, Y.; Guo, Z.; Yu, J.; Chen, Z.; Gao, J.; Yang, Y.; Qian, G.; Chen, B., A luminescent mixed-lanthanide metal-organic framework thermometer. *J Am Chem Soc* **2012**, *134* (9), 3979-82.
97. Cui, Y.; Yue, Y.; Qian, G.; Chen, B., Luminescent Functional Metal-Organic Frameworks. *Chem Rev* **2012**, *112* (2), 1126-1162.
98. Lan, A.; Li, K.; Wu, H.; Olson, D. H.; Emge, T. J.; Ki, W.; Hong, M.; Li, J., A Luminescent Microporous Metal-Organic Framework for the Fast and Reversible Detection of High Explosives. *Angewandte Chemie International Edition* **2009**, *48* (13), 2334-2338.
99. Fang, Q.; Zhu, G.; Xue, M.; Sun, J.; Sun, F.; Qiu, S., Structure, Luminescence, and Adsorption Properties of Two Chiral Microporous Metal-Organic Frameworks. *Inorganic Chemistry* **2006**, *45* (9), 3582-3587.
100. Pramanik, S.; Zheng, C.; Zhang, X.; Emge, T. J.; Li, J., New Microporous Metal-Organic Framework Demonstrating Unique Selectivity for Detection of High Explosives and Aromatic Compounds. *Journal of the American Chemical Society* **2011**, *133* (12), 4153-4155.
101. Naguib, M.; Gogotsi, Y., Synthesis of Two-Dimensional Materials by Selective Extraction. *Accounts of Chemical Research* **2015**, *48* (1), 128-135.
102. Ding, Y.; Chen, Y.-P.; Zhang, X.; Chen, L.; Dong, Z.; Jiang, H.-L.; Xu, H.; Zhou, H.-C., Controlled Intercalation and Chemical Exfoliation of Layered Metal-Organic Frameworks Using a Chemically Labile Intercalating Agent. *Journal of the American Chemical Society* **2017**, *139* (27), 9136-9139.
103. Niu, L.; Coleman, J. N.; Zhang, H.; Shin, H.; Chhowalla, M.; Zheng, Z., Production of Two-Dimensional Nanomaterials via Liquid-Based Direct Exfoliation. *Small* **2016**, *12* (3), 272-293.
104. Xiao, Y.; Cui, Y.; Zheng, Q.; Xiang, S.; Qian, G.; Chen, B., A microporous luminescent metal-organic framework for highly selective and sensitive sensing of Cu²⁺ in aqueous solution. *Chemical Communications* **2010**, *46* (30), 5503-5505.
105. Melber, C.; Keller, D.; Mangelsdorf, I.; International Programme on Chemical, S., Palladium. World Health Organization: Geneva, 2002.
106. Kumar, P.; Kumar, V.; Gupta, R., Selective fluorescent turn-off sensing of Pd²⁺ ion: applications as paper strips, polystyrene films, and in cell imaging. *RSC Advances* **2017**, *7* (13), 7734-7741.

107. Sanda, S.; Parshamoni, S.; Biswas, S.; Konar, S., Highly selective detection of palladium and picric acid by a luminescent MOF: a dual functional fluorescent sensor. *Chemical Communications* **2015**, *51* (30), 6576-6579.
108. Li, H.; Fan, J.; Hu, M.; Cheng, G.; Zhou, D.; Wu, T.; Song, F.; Sun, S.; Duan, C.; Peng, X., Highly sensitive and fast-responsive fluorescent chemosensor for palladium: reversible sensing and visible recovery. *Chemistry (Weinheim an der Bergstrasse, Germany)* **2012**, *18* (39), 12242-50.
109. Garrett, C. E.; Prasad, K., The Art of Meeting Palladium Specifications in Active Pharmaceutical Ingredients Produced by Pd-Catalyzed Reactions. *Advanced Synthesis & Catalysis* **2004**, *346* (8), 889-900.
110. Li, H.; Fan, J.; Du, J.; Guo, K.; Sun, S.; Liu, X.; Peng, X., A fluorescent and colorimetric probe specific for palladium detection. *Chemical Communications* **2010**, *46* (7), 1079-1081.
111. Zhao, M.; Yao, Z.-Q.; Xu, Y.-L.; Chang, Z.; Bu, X.-H., Guest dependent structure and acetone sensing properties of a 2D Eu³⁺ coordination polymer. *RSC Advances* **2017**, *7* (4), 2258-2263.
112. Zhao, S.-N.; Wang, G.; Poelman, D.; Voort, P. V. D., Luminescent Lanthanide MOFs: A Unique Platform for Chemical Sensing. *Materials (Basel)* **2018**, *11* (4), 572.
113. Chen, B.; Yang, Y.; Zapata, F.; Lin, G.; Qian, G.; Lobkovsky, E. B., Luminescent Open Metal Sites within a Metal–Organic Framework for Sensing Small Molecules. *Advanced Materials* **2007**, *19* (13), 1693-1696.
114. Zhang, Q.; Wang, J.; Kirillov, A. M.; Dou, W.; Xu, C.; Xu, C.; Yang, L.; Fang, R.; Liu, W., Multifunctional Ln–MOF Luminescent Probe for Efficient Sensing of Fe³⁺, Ce³⁺, and Acetone. *ACS Applied Materials & Interfaces* **2018**, *10* (28), 23976-23986.
115. Zhang, X.-J.; Su, F.-Z.; Chen, D.-M.; Peng, Y.; Guo, W.-Y.; Liu, C.-S.; Du, M., A water-stable EuIII-based MOF as a dual-emission luminescent sensor for discriminative detection of nitroaromatic pollutants. *Dalton Transactions* **2019**, *48* (5), 1843-1849.
116. Yang, L.; Powell, D. R.; Houser, R. P., Structural variation in copper(i) complexes with pyridylmethylamide ligands: structural analysis with a new four-coordinate geometry index, τ_4 . *Dalton Transactions* **2007**, (9), 955-964.
117. Marlin, D. S.; Olmstead, M. M.; Mascharak, P. K., Structure–Spectroscopy Correlation in Distorted Five-Coordinate Cu(II) Complexes: A Case Study with a Set of Closely Related Copper Complexes of Pyridine-2,6-dicarboxamide Ligands. *Inorganic Chemistry* **2001**, *40* (27), 7003-7008.
118. Guo, Z.; Xu, H.; Su, S.; Cai, J.; Dang, S.; Xiang, S.; Qian, G.; Zhang, H.; O’Keeffe, M.; Chen, B., A robust near infrared luminescent ytterbium metal–organic framework for sensing of small molecules. *Chemical Communications* **2011**, *47* (19), 5551-5553.
119. Yang, W.; Feng, J.; Zhang, H., Facile and rapid fabrication of nanostructured lanthanide coordination polymers as selective luminescent probes in aqueous solution. *Journal of Materials Chemistry* **2012**, *22* (14), 6819-6823.
120. Yi, F.-Y.; Yang, W.; Sun, Z.-M., Highly selective acetone fluorescent sensors based on microporous Cd(ii) metal–organic frameworks. *Journal of Materials Chemistry* **2012**, *22* (43), 23201-23209.
121. Parmar, B.; Rachuri, Y.; Bisht, K. K.; Suresh, E., Mixed-Ligand LMOF Fluorosensors for Detection of Cr(VI) Oxyanions and Fe³⁺/Pd²⁺ Cations in Aqueous Media. *Inorganic Chemistry* **2017**, *56* (18), 10939-10949.

122. Helal, A.; Nguyen, H. L.; Al-Ahmed, A.; Cordova, K. E.; Yamani, Z. H., An Ultrasensitive and Selective Metal–Organic Framework Chemosensor for Palladium Detection in Water. *Inorganic Chemistry* **2019**, *58* (3), 1738-1741.
123. van Middlesworth, J. M.; Wood, S. A., The stability of palladium(II) hydroxide and hydroxy–chloride complexes: an experimental solubility study at 25–85°C and 1 bar. *Geochimica et Cosmochimica Acta* **1999**, *63* (11), 1751-1765.
124. Balamurugan, R.; Liu, J.-H.; Liu, B.-T., A review of recent developments in fluorescent sensors for the selective detection of palladium ions. *Coordination Chemistry Reviews* **2018**, *376*, 196-224.
125. Wei, C.; He, Y.; Shi, X.; Song, Z., Terpyridine-metal complexes: Applications in catalysis and supramolecular chemistry. *Coordination Chemistry Reviews* **2019**, *385*, 1-19.
126. Fache, F.; Schulz, E.; Tommasino, M. L.; Lemaire, M., Nitrogen-containing ligands for asymmetric homogeneous and heterogeneous catalysis. *Chem Rev* **2000**, *100* (6), 2159-2231.
127. Deiters, A.; Martin, S. F., Synthesis of oxygen- and nitrogen-containing heterocycles by ring-closing metathesis. *Chem Rev* **2004**, *104* (5), 2199-2238.
128. Chelucci, G.; Thummel, R. P., Chiral 2,2' -bipyridines, 1,10-phenanthrolines, and 2,2' :6' ,2'' -terpyridines: Syntheses and applications in asymmetric homogeneous catalysis. *Chem Rev* **2002**, *102* (9), 3129-3170.
129. Winter, A.; Newkome, G. R.; Schubert, U. S., Catalytic Applications of Terpyridines and their Transition Metal Complexes. *ChemCatChem* **2011**, *3* (9), 1384-1406.
130. Lv, H.; Rudd, J. A.; Zhuk, P. F.; Lee, J. Y.; Constable, E. C.; Housecroft, C. E.; Hill, C. L.; Musaev, D. G.; Geletii, Y. V., Bis(4' -(4-pyridyl)-2,2' :6' ,2' ' -terpyridine)ruthenium(ii) complexes and their N-alkylated derivatives in catalytic light-driven water oxidation. *RSC Advances* **2013**, *3* (43), 20647-20654.
131. Hofmeier, H.; Schubert, U. S., Recent developments in the supramolecular chemistry of terpyridine–metal complexes. *Chemical Society Reviews* **2004**, *33* (6), 373-399.
132. Paul, A.; Ribeiro, A. P. C.; Karmakar, A.; Guedes da Silva, M. F. C.; Pombeiro, A. J. L., A Cu(ii) MOF with a flexible bifunctionalised terpyridine as an efficient catalyst for the single-pot hydrocarboxylation of cyclohexane to carboxylic acid in water/ionic liquid medium. *Dalton Transactions* **2016**, *45* (32), 12779-12789.
133. Young, D. C.; Yang, H.; Telfer, S. G.; Kruger, P. E., An Isoreticular Series of Zinc(II) Metal–Organic Frameworks Derived from Terpyridylcarboxylate Ligands. *Inorganic Chemistry* **2017**, *56* (20), 12224-12231.
134. Lin, Z.; Thacker, N. C.; Sawano, T.; Drake, T.; Ji, P.; Lan, G.; Cao, L.; Liu, S.; Wang, C.; Lin, W., Metal–organic layers stabilize earth-abundant metal–terpyridine diradical complexes for catalytic C–H activation. *Chemical Science* **2018**, *9* (1), 143-151.
135. Xiong, Y.; Gao, Y.; Guo, X.; Wang, Y.; Su, X.; Sun, X., Water-Stable Metal–Organic Framework Material with Uncoordinated Terpyridine Site for Selective Th(IV)/Ln(III) Separation. *ACS Sustainable Chemistry & Engineering* **2019**, *7* (3), 3120-3126.
136. Zhang, Y.; Li, J.; Yang, X.; Zhang, P.; Pang, J.; Li, B.; Zhou, H.-C., A mesoporous NNN-pincer-based metal–organic framework scaffold for the preparation of noble-metal-free catalysts. *Chemical Communications* **2019**, *55* (14), 2023-2026.

137. Chen, H.; Fan, P.; Tu, X.; Min, H.; Yu, X.; Li, X.; Zeng, J.-L.; Zhang, S.; Cheng, P., A Bifunctional Luminescent Metal-Organic Framework for the Sensing of Paraquat and Fe³⁺ Ions in Water. *CHEMISTRY-AN ASIAN JOURNAL* **2019**, *14* (20), 3611-3619.
138. Hunter, C. A.; Sanders, J. K. M., The nature of π - π interactions. *Journal of the American Chemical Society* **1990**, *112* (14), 5525-5534.